NASA TECHNICAL NOTE

NASA TN D-8366

THE THEORETICAL REFLECTANCE OF X-RAYS FROM OPTICAL SURFACES

John R. Neergaard, John M. Reynolds, and Stanley A. Fields

George C. Marshall Space Flight Center
Marshall Space Flight Center, Ala. 35812

NATIONAL AERONAUTICS AND SPACE ADMINISTRATION • WASHINGTON, D. C. • NOVEMBER 1976

1. REPORT NO.	2. GOVERNMENT ACCESSION NO.	3. RECIPIENT'S CATALOG NO.
NASA TN D-8366		

4. TITLE AND SUBTITLE	5. REPORT DATE
The Theoretical Reflectance of X-Rays from Optical Surfaces	November 1976
	6. PERFORMING ORGANIZATION CODE

7. AUTHOR(S)	8. PERFORMING ORGANIZATION REPORT #
John R. Neergaard,* John M. Reynolds, and Stanley A. Fields	M-195

9. PERFORMING ORGANIZATION NAME AND ADDRESS	10. WORK UNIT NO.
George C. Marshall Space Flight Center Marshall Space Flight Center, Alabama 35812	11. CONTRACT OR GRANT NO.
	13. TYPE OF REPORT & PERIOD COVERED
12. SPONSORING AGENCY NAME AND ADDRESS	Technical Note
National Aeronautics and Space Administration Washington, D.C. 20546	14. SPONSORING AGENCY CODE

15. SUPPLEMENTARY NOTES

Prepared by Space Sciences Laboratory, Science and Engineering
*NAS Postdoctoral Fellow.

16. ABSTRACT

The theoretical reflectance of X-rays from various materials and evaporated films is presented. A computer program has been written that computes the reflected intensity as a function of the angle of the incident radiation. The quantities necessary to generate the efficiency and their effect on the data are demonstrated. Five materials were chosen for evaluation: (1) fused silica, (2) chromium, (3) beryllium, (4) gold, and (5) a thin layer contaminant. Fused silica is a versatile and common material; chromium has high reflection efficiency at X-ray wavelengths and is in the middle of the atomic number range; beryllium contains a single atomic shell and has a low range atomic number; gold contains multiple atomic shells and has a high atomic number; the contaminant is treated as a thin film in the calculations and results are given as a function of thickness for selected wavelengths. The theoretical results are compared to experimental data at $\lambda = 8.34$ Å.

17. KEY WORDS	18. DISTRIBUTION STATEMENT
	Category 74

19. SECURITY CLASSIF. (of this report)	20. SECURITY CLASSIF. (of this page)	21. NO. OF PAGES	22. PRICE
Unclassified	Unclassified	55	

*For sale by the National Technical Information Service, Springfield, Virginia 22161

TABLE OF CONTENTS

LIST OF ILLUSTRATIONS

LIST OF ILLUSTRATIONS (Continued)

LIST OF ILLUSTRATIONS (Continued)

LIST OF ILLUSTRATIONS (Concluded)

LIST OF TABLES

THE THEORETICAL REFLECTANCE OF X-RAYS FROM OPTICAL SURFACES

INTRODUCTION

The theoretical reflectance of X-rays from various materials and evaporated films has been published by several authors. This report presents some theoretical X-ray reflectance data for 0.711 Å to 113 Å. Five materials were selected for study: fused silica, chromium, beryllium, gold, and a thin layer contaminant on fused silica. The theoretical results are compared to experimental data for $\lambda = 8.34$ Å.

PRINCIPLE OF REFLECTION

The theory of X-ray reflectance from a surface is described by the Fresnel equations, and a derivation is given by Compton and Allison [1]. A useful form of the Fresnel equations is given in equations (1), (2), and (3), and the notations are those of Parratt [2]. The refractive index, r, for X-rays is calculated as follows:

$$r = 1 - (\delta + i\beta) \quad , \tag{1}$$

where

$$\delta = c\lambda^2 \left[Z + \sum_q g_q \, \mathrm{Re} \left[J_q \left(\frac{\lambda}{\lambda_q} \right) - 1 \right] \right] , \tag{2}$$

where

δ = deviation from unity of the real part of the index of refraction

Z = atomic number

λ = wavelength of incident radiation

q = particular electronic energy level

λ_q = wavelength of the qth absorption edge

g_q = qth oscillator strength

c = constant

Re = $[J_q(\lambda/\lambda_q) - 1]$ [see equation (8)] ,

and

$$\beta = \frac{\lambda}{4\pi}\mu \quad , \tag{3}$$

where β is the deviation from unity of the imaginary part of the index refraction and μ is the linear absorption coefficient.

Since the theory of X-ray reflectance models is well defined in the literature, only a few equations of interest will be presented here for comparison purposes to differentiate between the methods of approach available and that which was chosen for this report.

A general form for calculating the deviation from unity, δ, of the real part of the X-ray index of refraction [see equation (2)] is given in equation (4),

$$\delta = \left(\frac{\lambda^2 e^2}{2\pi m C^2}\right) \sum_a N_a (Z_a + \Delta f_a) \quad , \tag{4}$$

where

a = individual atomic species present

e = electronic charge

m = electronic mass

C = velocity of light

N = Avogadro's number

Δf_a = shell term correction to model independent approach.

It may be pointed out that an implication of equation (4) is uniform composition, at least insofar as the proportional number of atomic X-ray interactions is concerned. For the most part, such a lack of uniformity is experimentally insignificant and thus ignored. A possible exception might be a dynamic oxidation process in which the stoichiometry of the oxide is a function of time or position or both, or is a function of the spatial variation of a chemically uniform or, in some cases, chemically nonuniform contaminant.

The principal simplifying assumption, utilized primarily for ease of calculation in the literature (e.g., References 3 and 4), involves setting

$$\Delta f_a = 0 \quad . \tag{5}$$

This assumption is essentially a model independent approximation that is expected to be valid for energies far beyond resonance. This assumption has not been utilized in this report and implies expected reflection efficiency variations from those authors who used this assumption.

Tables 1 and 2 present dispersion calculations for fused silica and demonstrate the potential for reflection efficiency variations where $\Delta f_a \neq 0$. In the tables for the chosen model parameters, a comparison may be obtained for $\Delta f_a = 0$ and $\Delta f_a \neq 0$. The value in the last column of Tables 1 and 2 is the value associated with each shell of the atom in question, and the value inserted below the table is the value of Δf_a for the atom that is to be compared with Z to determine the effect of the shell term contribution upon the index of refraction. Specifically, the dependence of Δf_a upon the model parameters may be expressed in the form

$$\Delta f_a = \sum_q \Delta f_q \quad , \tag{6}$$

TABLE 1. DISPERSION CALCULATIONS FOR SILICON (Z = 14), λ = 8.34 Å

q [5]	λ_q (Å) [5]	λ/λ_q	P_q [2,6]	$Re[J_q(x) - 1]$	g_q [2,6]	$g_q\, Re(J_q - 1)$
K	6.74	1.237	2.75	-1.5710	1.45	-2.278
L_I	83.20	1.002×10^{-1}	2.0	-1.007×10^{-2}	1.55	-0.1562×10^{-1}
$L_{II\,III}$	124	6.725×10^{-2}	2.5	2.750×10^{-2}	5.00	0.1375
M_I	1550	5.38×10^{-3}	2.5	8.430×10^{-3}	2.00	0.1686×10^{-2}
$M_{II\,III}$	4130	2.019×10^{-3}	2.5	2.015×10^{-3}	2.00	0.4031×10^{-3}

$$\Delta f_a = \sum_q g_q \, Re[J_q(P_q; x) - 1] \simeq -2.154$$

TABLE 2. DISPERSION CALCULATIONS FOR OXYGEN (Z = 8), λ = 8.34 Å

q [5]	λ_q (Å) [5]	λ/λ_q	P_q [2,6]	$Re[J_q(x) - 1]$	g_q [2,6]	$g_q\, Re(J_q - 1)$
K	23.4	3.564×10^{-1}	2.75	1.883×10^{-1}	1.55	0.2919
L_I	518.0	1.610×10^{-2}	2.0	-2.592×10^{-3}	1.60	-0.4147×10^{-3}
$L_{II\,III}$	1780.0	4.685×10^{-3}	2.5	6.896×10^{-3}	5.40	0.3724×10^{-2}

$$\Delta f_a = \sum_q g_q \, Re[J_q(P_q; x) - 1] \simeq 0.2952 \times 10^{-1}$$

where

$$\Delta f_q = g_q \, \mathrm{Re}[J_q(P_q; x) - 1] \quad , \tag{7}$$

where

q = particular shell in question (e.g., K, L, etc. [5])

g = oscillator strength of particular shell

P = empirical wavelength power law exponent

x = ratio of incident wavelength to shell resonance wavelength

and

$$J_q = \frac{\alpha}{1 - ih} \int_0^1 \frac{y^{\alpha} \, dy}{y - \xi} \quad , \tag{8}$$

where

$\alpha = 1/2 \, (P_q - 1)$

$y = \omega_q / \omega'$ = inverse of ratio on integration variable to shell resonance frequency

h = related to radiation damping term [6]

$\xi = (\omega_q / \omega)^2 (1/1 - ih)$.

Arbitrary variations of the shell oscillator strength and power law exponent result in multiple values for δ, the real part of the index of refraction. Because of the potential multiplicity of P and q in equation (7) and because of the variation in literature values used, it is necessary to look further into the origin of the harmonic oscillator model parameters. Cromer summarizes the developmental history of the dispersion term [equation (4)] and finds general agreement with Parratt's earlier work [2,7].

The power law relating the mass absorption coefficient to frequency of incident X-radiation is regarded basically as an empirical formulation. One form of the law is

$$\mu_q(\omega) = \left(\frac{\omega_q}{\omega}\right)^{P_q} \mu_q(\omega_q) \quad , \tag{9}$$

when $\omega > \omega_q$, and when $\omega < \omega_q$,

$$\mu_q(\omega) = 0 \quad ,$$

where

$\mu_q(\omega)$ = absorption coefficient associated with qth shell

q = resonance frequency of qth shell

ω = incident frequency of X-radiation

$\mu_q(\omega_q)$ = absorption coefficient of shell q at frequency ω_q.

A lack of strict validity can be seen in the concept that $\mu(\omega) = 0$ for $\omega < \omega_q$, from which it can be inferred that no absorption takes place by an electron of the q shell unless the incident radiation energy exceeds the binding energy of the q shell electron. Further, a precise evaluation of $\mu_q(\omega)$ is

difficult due either to inherent experimental and/or theoretical problems, and, lastly, the power law exponent, P_q, is actually a function of incident frequency, i.e.,

$$P_q = P_q(\omega) \tag{10}$$

and is therefore not a constant as is typically used in the literature. The atomic shells and the exponents used for the given shells of fused silica are presented in Table 3.

At 8.34 Å the shell absorption coefficient was changed by approximately 10 percent plus $(+\Delta P_q)$ and minus $(-\Delta P_q)$ from the published literature values for silicon and oxygen. The results from these changes are indicated in the shell term, atom term, delta (δ), and the delta sum in Table 3 and Figures 1 and 2. It appears that when P_q is increased in value, there is a smaller change in δ than when the exponent is decreased. As the binding energy of the atomic shells decreases from the K to the L shell, the influence on δ is also decreased because of the change in ratio of λ/λ_q for the differing shells. Because the change in λ is small, these changes may be considered negligible since the differences in the reflection efficiency curve will be negligible.

The quantum mechanical oscillator strength applicable to X-ray reflection theory is often introduced in the literature by analogy to the classical mechanic harmonic oscillator. In this sense the calculation of the oscillator strengths followed the development of quantum mechanical techniques, as indeed the refinements in values obtained for the oscillator strength followed the development of quantum mechanical wave function approximation techniques, Hamiltonian refinements and additions, and the availability of computational facilities, apparently culminating in a self-consistent field relativistic "Dirac-Slater" wave function approach [7]. These oscillator strength values obtained by D. T. Cromer [7] appear to be the most accurate and have been utilized, when available, in this report. In general, there is good consistency among those authors who have calculated oscillator strengths, at least to the extent possible in terms of the method of approach (Hamiltonian assumptions).

TABLE 3. THE SHELL ABSORPTION COEFFICIENT P_q FOR FUSED SILICA, $\lambda = 8.34$ Å

Element	$-\Delta P_q$	New Shell Term	$+\Delta P_q$	New Shell Term	$-\Delta P_q$	New Shell Term	$+\Delta P_q$	New Shell Term	$-\Delta P_q$	New Shell Term	$+\Delta P_q$	New Shell Term	$-\Delta P_q$	New Shell Term	$+\Delta P_q$	New Shell Term
Silicon																
K-Abs. Edge . . . . . 6.74 Å																
Abs. Coeff . . P_q . . . 2.75	2.50	-2.199	3.0	-2.350												
Osc. Str 1.45																
Shell Term . . . . . -2.278																
L_I-Abs. Edge . . . . . 83.2 Å																
Abs. Coeff . . P_q . . . 2.0					1.8	-0.1109	2.2	0.3664×10^{-1}								
Osc. Str 1.55																
Shell Term . . -0.1562×10^{-1}																
$L_{II\ III}$-Abs. Edge . . . . 124.0 Å																
Abs. Coeff . . P_q 2.5									2.25	0.1015	2.75	0.1363				
Osc. Str 5.0																
Shell Term . . 0.1375																
Atom Term 0.1971	0.1984		0.1959		0.1954		0.1979		0.1964		0.1970					
Delta 0.7409×10^{-4}	0.7458×10^{-4}		0.7364×10^{-4}		0.7346×10^{-4}		0.7438×10^{-4}		0.7383×10^{-4}		0.7405×10^{-4}					
Oxygen																
K-Abs. Edge . . . . . 23.4 Å																
Abs. Coeff . . P_q . . . 2.75													2.50	0.1702	3.00	0.3795
Osc. Str 1.55																
Shell Term 0.2919																
L_I-Abs. Edge . . . . . 518 Å																
Abs. Coeff . . P_q 2.0					1.8	-0.2429×10^{-1}	2.2	0.6286×10^{-2}								
Osc. Str 1.6																
Shell Term . . -0.4147×10^{-3}																
$L_{II\ III}$-Abs. Edge . . . . . 1780 Å																
Abs. Coeff . . P_q . 2.5									2.25	0.5186×10^{-2}	2.75	0.2177×10^{-2}				
Osc. Str 5.4																
Shell Term -0.3724×10^{-2}																
Atom Term 0.2760	0.2760		0.2760		0.2752		0.2762		0.2760		0.2759		0.2719		0.2789	
Delta 0.1037×10^{-3}	0.1037×10^{-3}		0.1037×10^{-3}		0.1034×10^{-3}		0.1038×10^{-3}		0.1037×10^{-3}		0.1037×10^{-3}		0.1022×10^{-3}		0.1048×10^{-3}	
Delta Sum 0.1778×10^{-3}	0.1778×10^{-3}		0.1773×10^{-3}		0.1769×10^{-3}		0.1782×10^{-3}		0.1776×10^{-3}		0.1777×10^{-3}		0.1763×10^{-3}		0.1789×10^{-3}	

Shell Term: $g_q[\mathrm{Re}(J_q - 1)]$ Atom Term: $\frac{Z + \Sigma \text{ shell term}}{\text{atomic weight}}$

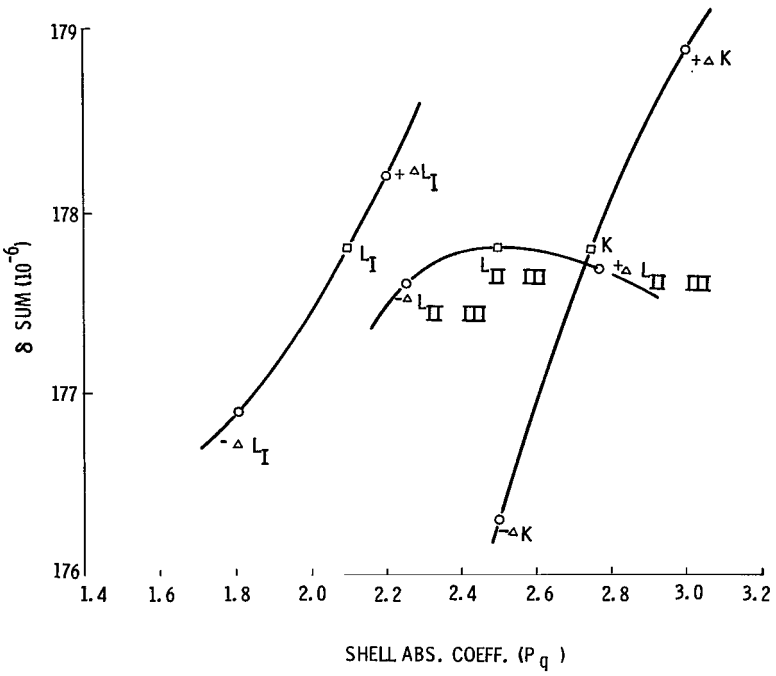

Figure 1. Shell absorption coefficient (P_q) for oxygen, $\lambda = 8.34$ Å.

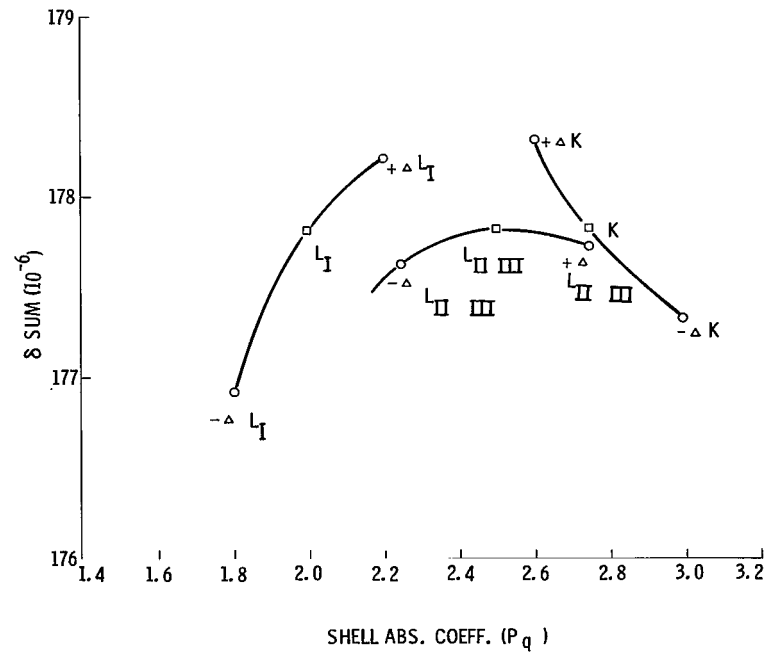

Figure 2. Shell absorption coefficient (P_q) for silicon, $\lambda = 8.34$ Å.

Again, fused silica was chosen as an example, and Table 4 is a list of the oscillator strengths at 8.34 Å [7]. The oscillator strength (g_q) was changed approximately 10 percent plus ($+\Delta g_q$) and minus ($-\Delta g_q$) from the values published in the literature [6]. Again, the change in δ is very small, as indicated in Figures 3 and 4, and in some cases there is no change. The K-absorption edge of silicon is 6.74 Å, which is relatively close to the wavelength of interest, 8.34 Å. Thus, the greatest change in δ occurs for the K shell when g_q of silicon is changed. The next nearest resonance is the K-absorption edge of oxygen at 23.4 Å. Consistent with equation (8), the contribution of this shell is smaller than that of the silicon K shell. Depending upon the value of the integral in equation (8) and more specifically the ratio of the shell resonance frequency to incident frequency, the calculated contribution of the shell to the index of refraction (and thus its contribution to the reflection efficiency) become insignificant, negating to some extent the effect of inaccuracies and inconsistencies in published oscillator strengths.

COMPUTATIONS

A program has been written that computes the reflected intensity as a function of the angle of incidence of an X-ray beam incident at grazing angles on a laminated planar surface [6]. The following data are necessary for use in the program to calculate the X-ray reflection at a given wavelength. References are given for the data used in this report.

Layer Parameters

1. Number of layers above the substrate
2. Layer thickness
3. Layer material density [8]

Atomic Element Parameters

4. Number of chemical elements
5. Atomic number of the element [8]

TABLE 4. SHELL OSCILLATOR STRENGTH g_q FOR FUSED SILICA, $\lambda = 8.34$ Å

Element	$-\Delta g_q$	New Shell Term	$+\Delta g_q$	New Shell Term	$-\Delta g_q$	New Shell Term	$+\Delta g_q$	New Shell Term	$-\Delta g_q$	New Shell Term	$+\Delta g_q$	New Shell Term	$-\Delta g_q$	New Shell Term	$+\Delta g_q$	New Shell Term
Silicon																
K-Abs. Edge . . . . . 6.74 Å																
Abs. Coeff. 2.75																
Osc. Str . . . . g_q 1.45	1.30	-2.042	1.60	-2.514												
Shell Term . . . . . -2.278																
L_I-Abs. Edge . . . . . 83.2 Å																
Abs. Coeff 2.0																
Osc. Str . . . . g_q 1.55					1.40	-0.1411×10^{-1}	1.70	-0.1713×10^{-1}								
Shell Term . . . -0.1562×10^{-1}																
$L_{II\ III}$-Abs. Edge . . . . . 124 Å																
Abs. Coeff 2.5																
Osc. Str . . . . g_q . . . 5.0									4.5	0.1238	5.5	0.1513				
Shell Term 0.1375																
Atom Term 0.1971	0.2010		0.1931		0.1970		0.1970		0.1968		0.1972					
Delta 0.7409×10^{-4}	0.7556×10^{-4}		0.7261×10^{-4}		0.7406×10^{-4}		0.7405×10^{-4}		0.7397×10^{-4}		0.7414×10^{-4}					
Oxygen																
K-Abs. Edge . . . . . 23.4 Å																
Abs. Coeff 2.75																
Osc. Str . . . . g_q 1.55													1.40	0.2637	1.70	0.3202
Shell Term 0.2919																
L_I-Abs. Edge . . . . . 518 Å																
Abs. Coeff 2.0																
Osc. Str . . . . g_q 1.6					1.45	0.3759×10^{-3}	1.75	-0.4536×10^{-3}								
Shell Term . . . . -0.4147×10^{-3}																
$L_{II\ III}$-Abs. Edge . . . . . 1780 Å																
Abs. Coeff 2.5																
Osc. Str . . . . g_q . . 5.4									4.85	0.3345×10^{-2}	6.05	0.4173×10^{-2}				
Shell Term -0.3724×10^{-2}																
Atom Term 0.2760					0.2760		0.2760		0.2760		0.2760		0.2750		0.2769	
Delta 0.1037×10^{-3}					0.1037×10^{-3}		0.1037×10^{-3}		0.1037×10^{-3}		0.1037×10^{-3}		0.1033×10^{-3}		0.1041×10^{-3}	
Delta Sum 0.1778×10^{-3}	0.1793×10^{-3}		0.1763×10^{-3}		0.1778×10^{-3}		0.1778×10^{-3}		0.1777×10^{-3}		0.1779×10^{-3}		0.1774×10^{-3}		0.1781×10^{-3}	

Shell Term: $g_q[\mathrm{Re}(J_q - 1)]$ Atom Term: $\frac{Z + \Sigma \text{ shell term}}{\text{atomic weight}}$

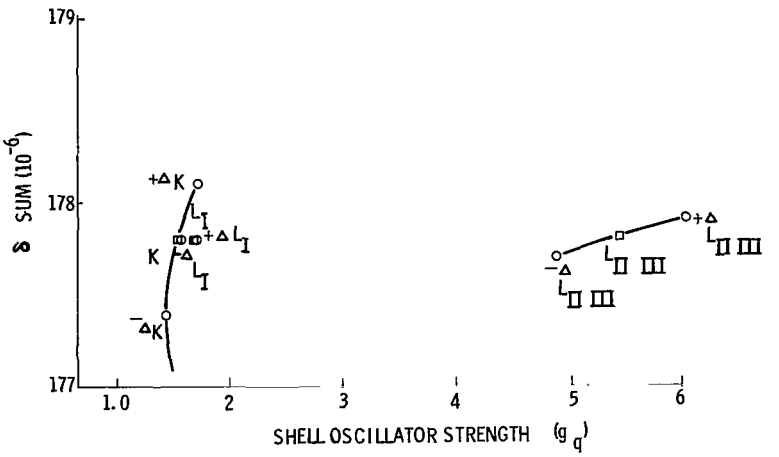

Figure 3. Shell oscillator strength (g_q) for oxygen, $\lambda = 8.34$ Å.

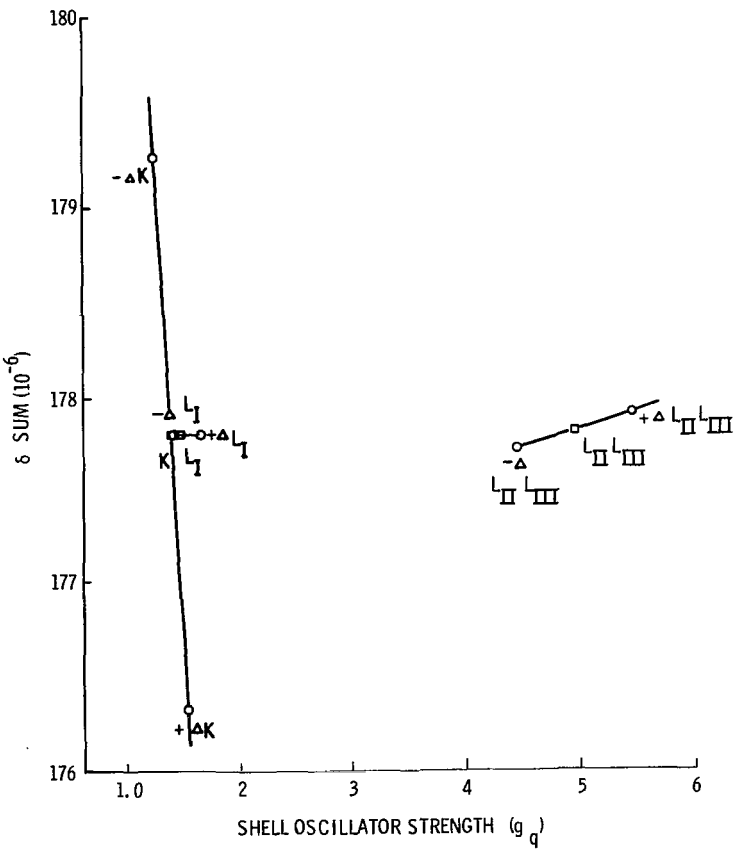

Figure 4. Shell oscillator strength (g_q) for silicon, $\lambda = 8.34$ Å.

6. Atomic weight of the element [8]

7. The element abundance

8. Mass absorption coefficient [9,10]

Atomic Shell Parameters

9. The number of atomic shells [5]

10. The shell absorption edge (λ_q) [5]

11. The shell absorption coefficient power law exponent (P_q) [5,7,11]

12. The shell oscillator strength (per atom g_q) [7,11].

The program calculates the real and imaginary components, δ and β, of the complex index of refraction and the reflectance at a given angle of incidence.

Fused Silica

Fused silica is a very common material used in the reflection of X-rays. The material is used as a reflector itself or as a substrate for deposition of thin films. From the input data described previously, the density might be varied to change the real and imaginary components of the index of refraction [equation (1)].

Deviation from the bulk density of the material is common for deposited materials, and deviations have been reported also for polished materials. These deviations must be given strong consideration when comparing experimental and theoretical results [12-18]. The theoretical reflection efficiency curves were calculated for fused silica having bulk densities of 2.0, 2.2, and 2.4 g/cm^3 and at a wavelength of 8.34 Å. The value of 2.0 g/cm^3 was chosen as symbolic of a possible surface density modification resulting from polishing. Other values for the bulk density of fused silica were selected because they are reasonable and also to demonstrate the effect of density variations on the reflection efficiency of a material. Figure 5 is a plot of the reflection efficiency as a function of the angle of incidence. Fused silica with a density of 2.0 g/cm^3 was selected as the best comparison of the theoretical results with experimental data (Fig. 6). Table 5 gives the tabulated values of β, δ, and the critical angle (θ_c) obtained with the density change in fused silica.

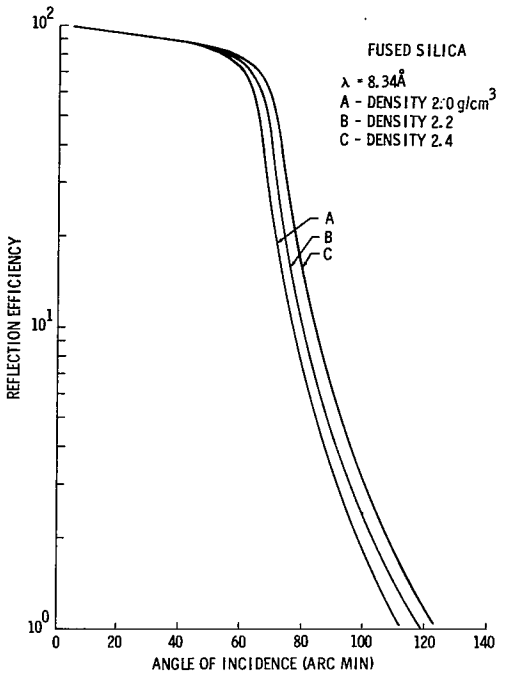

Figure 5. Reflection efficiency for fused silica, λ = 8.34 Å.

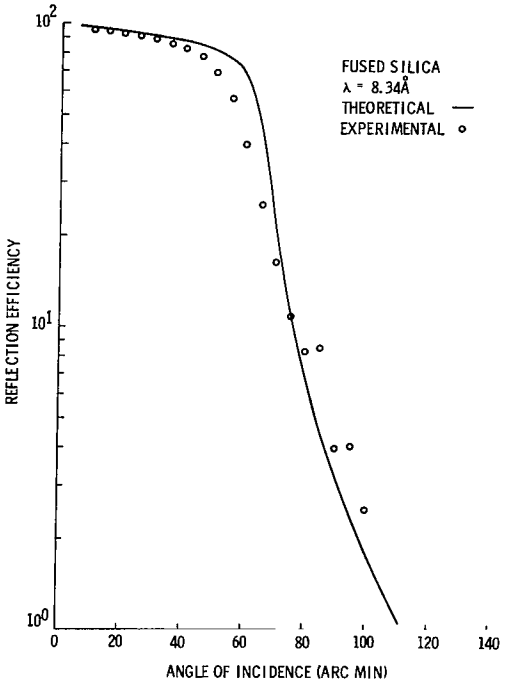

Figure 6. Theoretical and experimental reflection efficiency, λ = 8.34 Å.

TABLE 5. DENSITY VARIATION OF FUSED SILICA

Density (g/cm^3)	δ	β	Critical Angle, $\theta_c = \sqrt{2\rho}$ (min)
2.0	0.177×10^{-3}	0.145×10^{-4}	64.68
2.2	0.195×10^{-3}	0.160×10^{-4}	67.89
2.4	0.213×10^{-3}	0.175×10^{-4}	70.95

As the density of fused silica increases, so do the reflection efficiencies for a given angle of incidence, δ, β, and the critical angle. Scott [14] reports that in the region near the critical angle, for substrate density variations, the angle of incidence necessary to generate an identical reflection efficiency value can be approximated by the relation

$$\theta_c(\rho_2) = \theta_c(\rho_1)\sqrt{\frac{\rho_2}{\rho_1}} \quad , \tag{11}$$

where ρ_1 = first layer density and ρ_2 = second layer density. The structure similarity obtained in Figure 5 is generally valid in two-media systems where only a substrate density variation is allowed if incident X-rays of resonance energy are excluded.

Based on the previous comparison of the experimental and theoretical data at 8.34 Å and a density of 2.0 g/cm^3, a group of theoretical X-ray reflection efficiency curves were calculated in which only the wavelength varied. Figures 7 through 11 are the reflection efficiency curves as a function of the angle of incidence for the wavelengths of 1.54 Å to 113 Å. Figure 12 is a consolidation of these data with reflection efficiency as a function of wavelength for selected values of θ. Figure 13 is a presentation of θ_c, β/δ ratio, and the shell absorption edges for fused silica over this wavelength range.

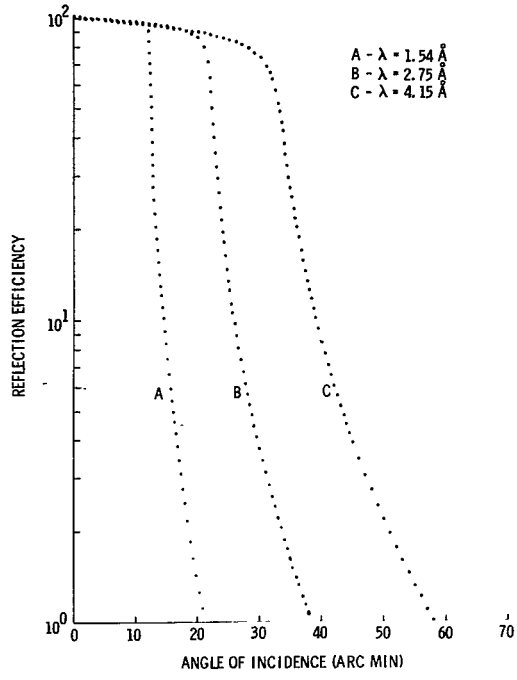

Figure 7. Reflection efficiency for fused silica, $\lambda = 1.54$ Å, 2.75 Å, and 4.15 Å.

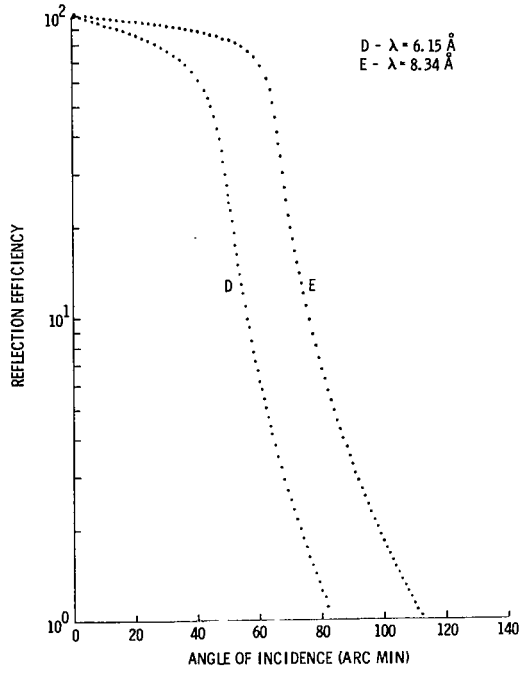

Figure 8. Reflection efficiency for fused silica, $\lambda = 6.15$ Å and 8.34 Å.

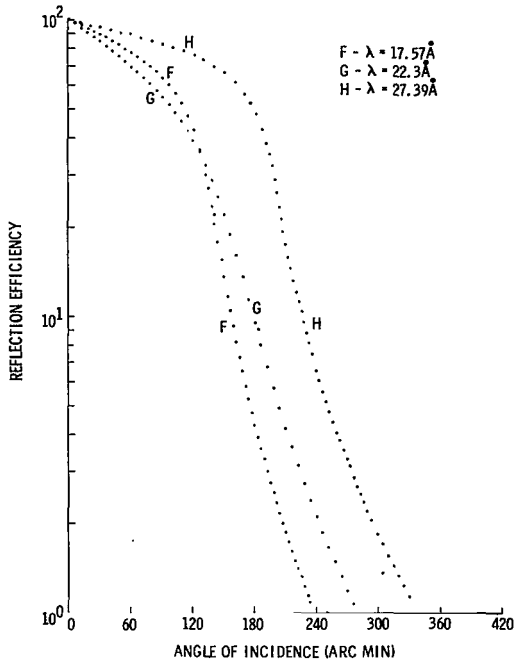

Figure 9. Reflection efficiency for fused silica, λ = 17.57 Å, 22.3 Å, and 27.39 Å.

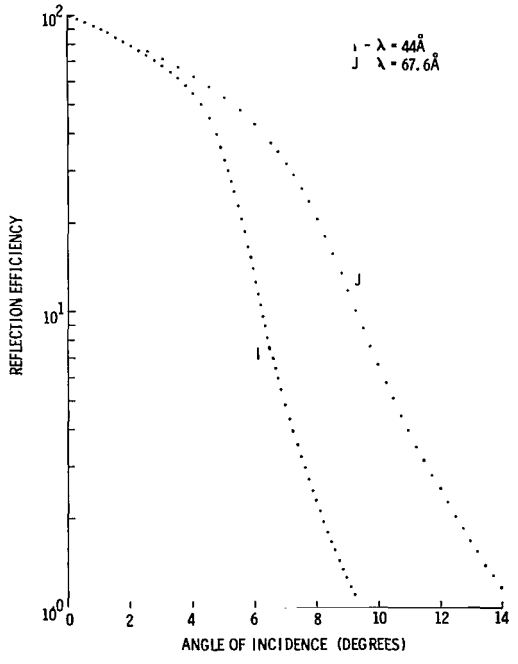

Figure 10. Reflection efficiency for fused silica, λ = 44 Å and 67.6 Å.

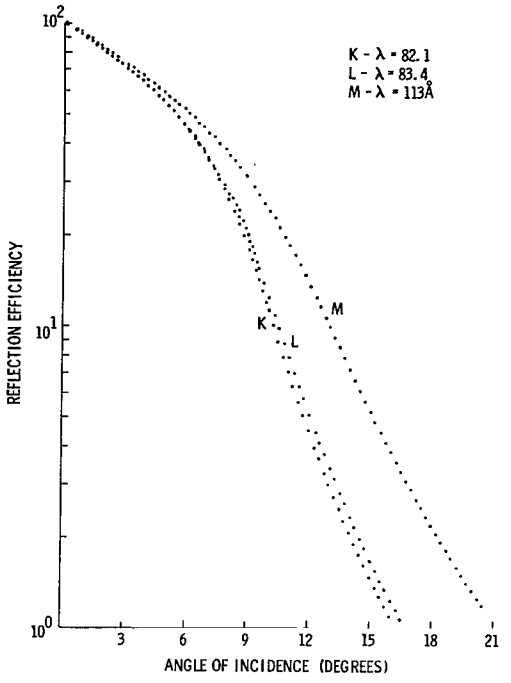

Figure 11. Reflection efficiency for fused silica, λ = 82.1 Å, 83.4 Å, and 113 Å.

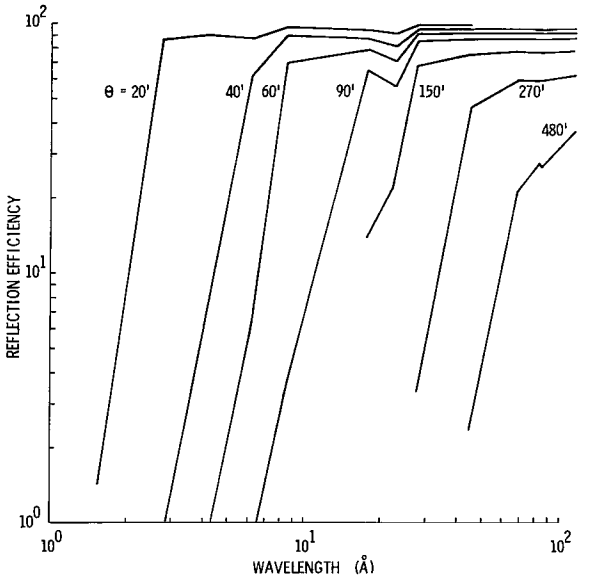

Figure 12. Theoretical reflection efficiency for fused silica, λ = 1.54 Å to 113 Å.

The influence of the atomic shell absorption edges is noticeable in Figures 12 and 13. In Figure 12 the oxygen K-edge (23.3 Å) is evident even at the smaller angles of incidence (20 min) and is even more evident at the larger angles of incidence (90 min). A comparison of the critical angle and the β/δ ratio in Figure 13 verifies the absorption edge influence. Silicon has two absorption edges, the K shell at 6.7 Å and the L_I shell at 83.4 Å. These two absorption edges of silicon verify the absorption effect even though it is not as apparent at longer wavelengths (83.4 Å).

Chromium

Chromium, with an atomic number of Z = 24 and several atomic shells, was the next material selected. For calculation purposes, chromium was assumed to be 1000 Å thick and deposited as a thin film on fused silica.

Individual calculations were performed on the chromium layer and the fused silica substrate for generation of δ and β, and standard interface techniques were applied utilizing an arbitrary definition of I_j/I_{j+1}, $K = 10^{-4}$ as the zero incident intensity [6], where I_j = the beam incident on an interface j, and I_{j+1} = the beam transmitted through the interface j + 1. When the 10^{-4} relative intensity ratio was reached, no further consideration was given to that part of the beam transmitted through interface j + 1. Three densities were chosen for theoretical calculations: 6.0, 7.14, and 8.0 g/cm^3. The density of a thin film is a result of the conditions of depositions and the metal itself. In the case of chromium, a density of 6.0 g/cm^3 appears to compare most favorably with the experimental data (Fig. 14).

Chromium was chosen as a material in order to examine the variation of the oscillator model parameters. The literature contains discussions as to the quantities to use for the oscillator strengths. The Thomas-Reiche-Kuhn summation rule states that for a one-electron atom,

$$g\left(\frac{k}{n}\right) = 1 \quad , \tag{12}$$

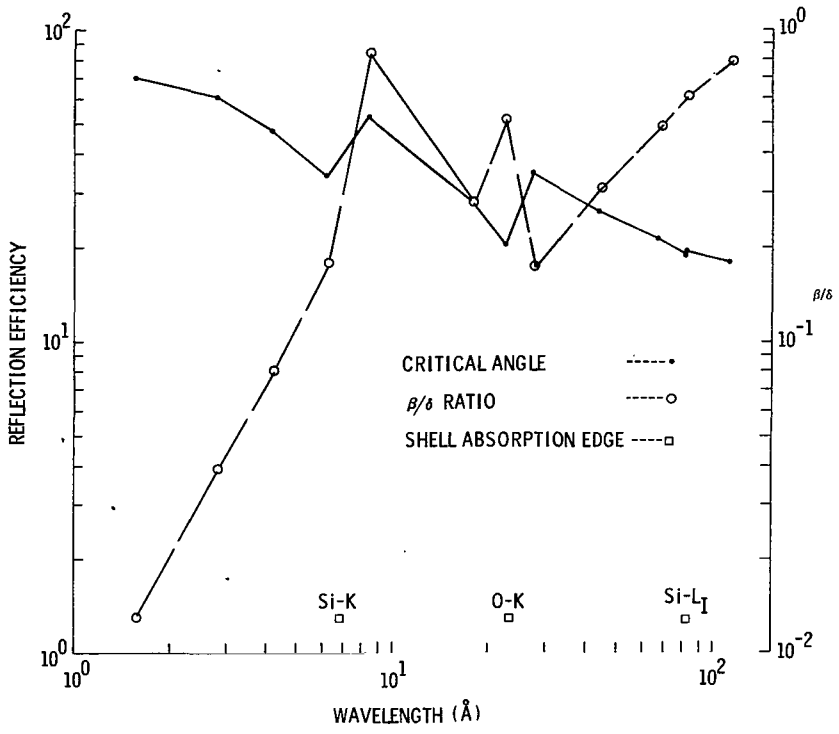

Figure 13. Critical angle, β/δ ratio, and shell absorption edge for fused silica, $\lambda = 1.54$ Å to 113 Å.

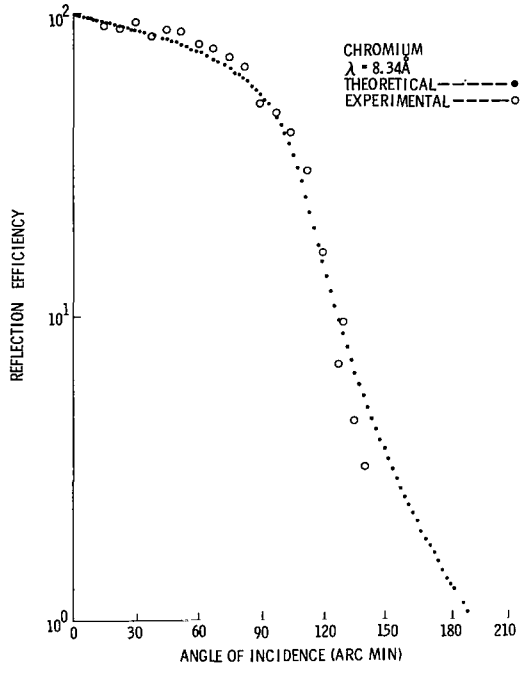

Figure 14. Theoretical and experimental reflection efficiency for chromium, $\lambda = 8.34$ Å.

and for a many-electron atom, the sum of the oscillator strengths is equal to Z, the atomic number [2,7,11]. Variations of adherence to the Thomas-Reiche-Kuhn summation rule and variations of the values chosen for the individual atomic shells exist in the literature.

From the literature, two examples were selected for various quantities of g_q, and these are tabulated in Table 6. Table 6 is an example of different oscillator strength numbers for chromium, Z = 24. Part A of the table represents P_q's and g_q's from Reference 7, and the information in part B was taken from Reference 6.

Three types of variation are present in Table 6. They are individual variation of P and g, simultaneous variation of P and g, and shell grouping. Although the individual variation of P and g most effectively differentiates reflection efficiency differences, simultaneous variations and different shell groupings are typical of comparison difficulties encountered in the literature.

Based on the comparison of experimental and theoretical results, curves were developed for $\lambda = 1.54$ Å to $\lambda = 113$ Å using those g_q's from Reference 7 (Figs. 15 through 17). The effect of the chromium L_{II} absorption edge at $\lambda = 21.4$ Å is demonstrated in Figure 16, curve G, with a drastic decrease in the reflection efficiency as λ is increased. Figure 18 is a consolidation of the individual wavelengths for selected values of θ and illustrates the absorption edge effect at 21.4 Å. Figure 19 shows the critical angles, β/δ ratios, and the shell absorption edges for chromium. The figures indicate the contribution of the shell absorption edges and the β/δ variation from wavelengths of 1.54 Å to 113 Å.

Beryllium

Beryllium is another common material with one atomic shell [8]. The grade and properties of beryllium were taken from those telescope materials used by NASA on the Apollo Telescope Mount [3]. The composition of the metal is: Be (98.49 percent), BeO (1.4 percent), C (0.081 percent), Fe (0.170 percent), Al (0.059 percent), Mg (0.021 percent), and Si (0.080 percent) (Table 7). All of these elements were included in the calculations for the

TABLE 6. ATOMIC SHELL PARAMETER OF CHROMIUM, $\lambda = 8.34$ Å

Element	q	λ_q(Å)	P_q	g_q	Shell Term	Atom Term
A. Cr	K	2.07	2.75	1.34	-1.380	
	L_I	17.85	2.33	1.37	-0.3760×10^{-1}	
	L_{II}	21.24	2.50	1.95	0.1980	
	L_{III}	21.58	2.50	4.41	0.4559	
	M_I	167.30	2.50	0.94	0.1763×10^{-1}	
	M_{II}, M_{III}	291.70	2.50	5.41	0.4835×10^{-1}	0.4481
					Delta Sum	0.5053×10^{-3}
B. Cr	K	2.07	2.75	1.33	-1.369	
	L_I	17.90	2.0	1.50	-0.3528	
	L_{II}, L_{III}	21.40	2.5	4.0	0.4098	
	M_I	168.00	2.5	1.7	0.3172×10^{-1}	
	M_{II}, M_{III}	288.00	2.5	5.0	0.4547×10^{-1}	
	M_{IV}, M_V	6200.00	2.5	9.0	0.9973×10^{-3}	0.4377
					Delta Sum	0.5874×10^{-3}

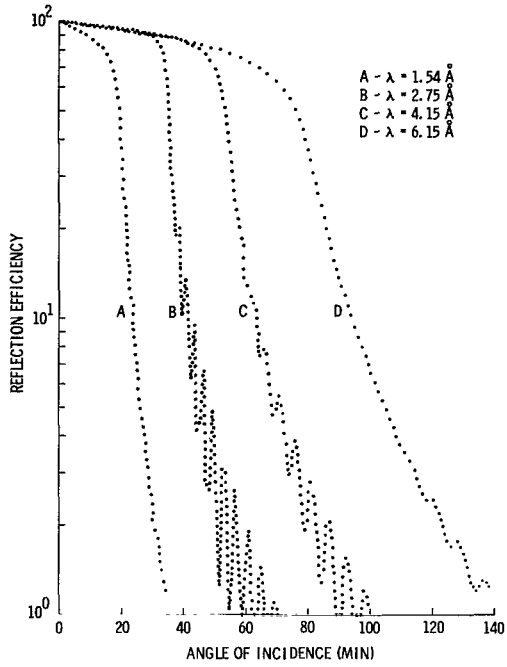

Figure 15. Reflection efficiency for chromium, λ = 1.54 Å, 2.75 Å, 4.15 Å, and 6.15 Å.

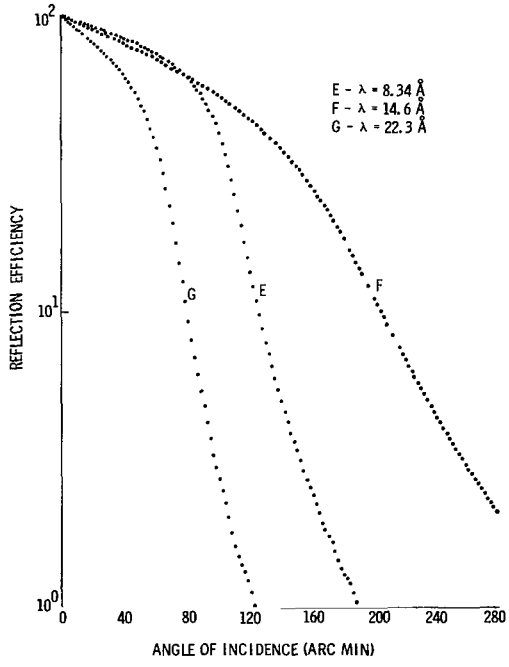

Figure 16. Reflection efficiency for chromium, λ = 8.34 Å, 14.6 Å, and 22.3 Å.

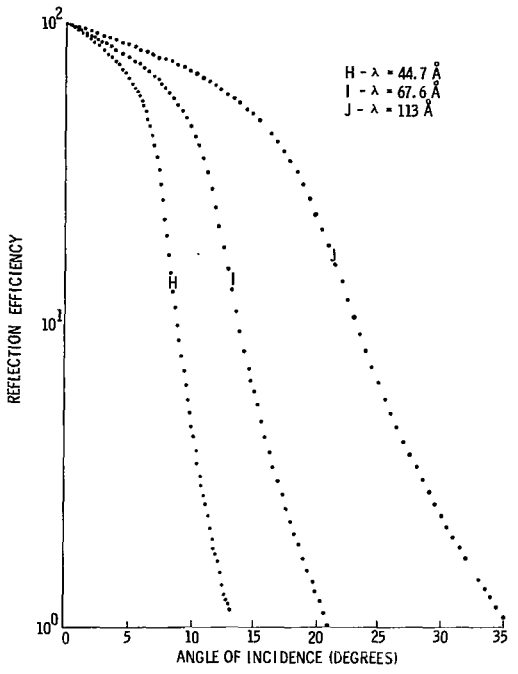

Figure 17. Reflection efficiency for chromium, λ = 44.7 Å, 67.6 Å, and 113 Å.

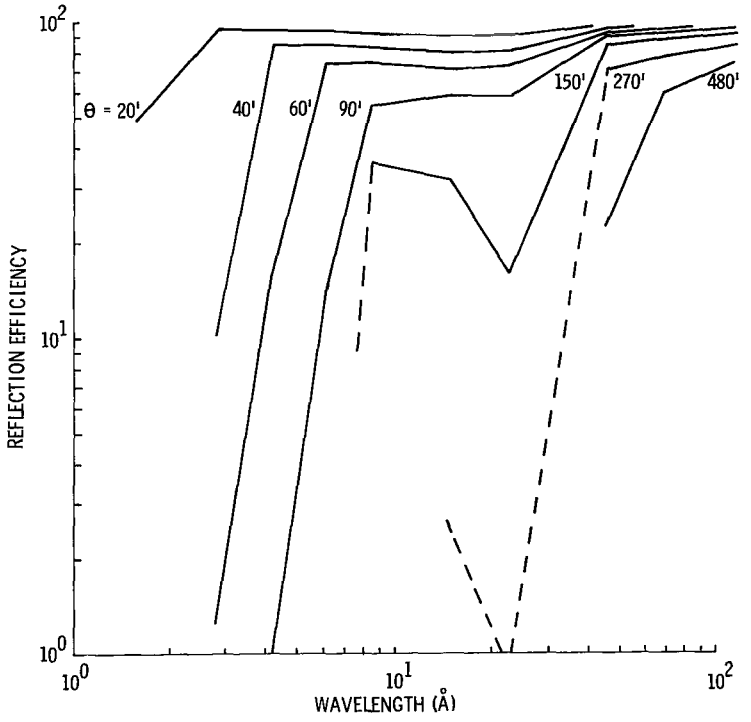

Figure 18. Theoretical reflection efficiency for chromium, λ = 1.54 Å to 113 Å.

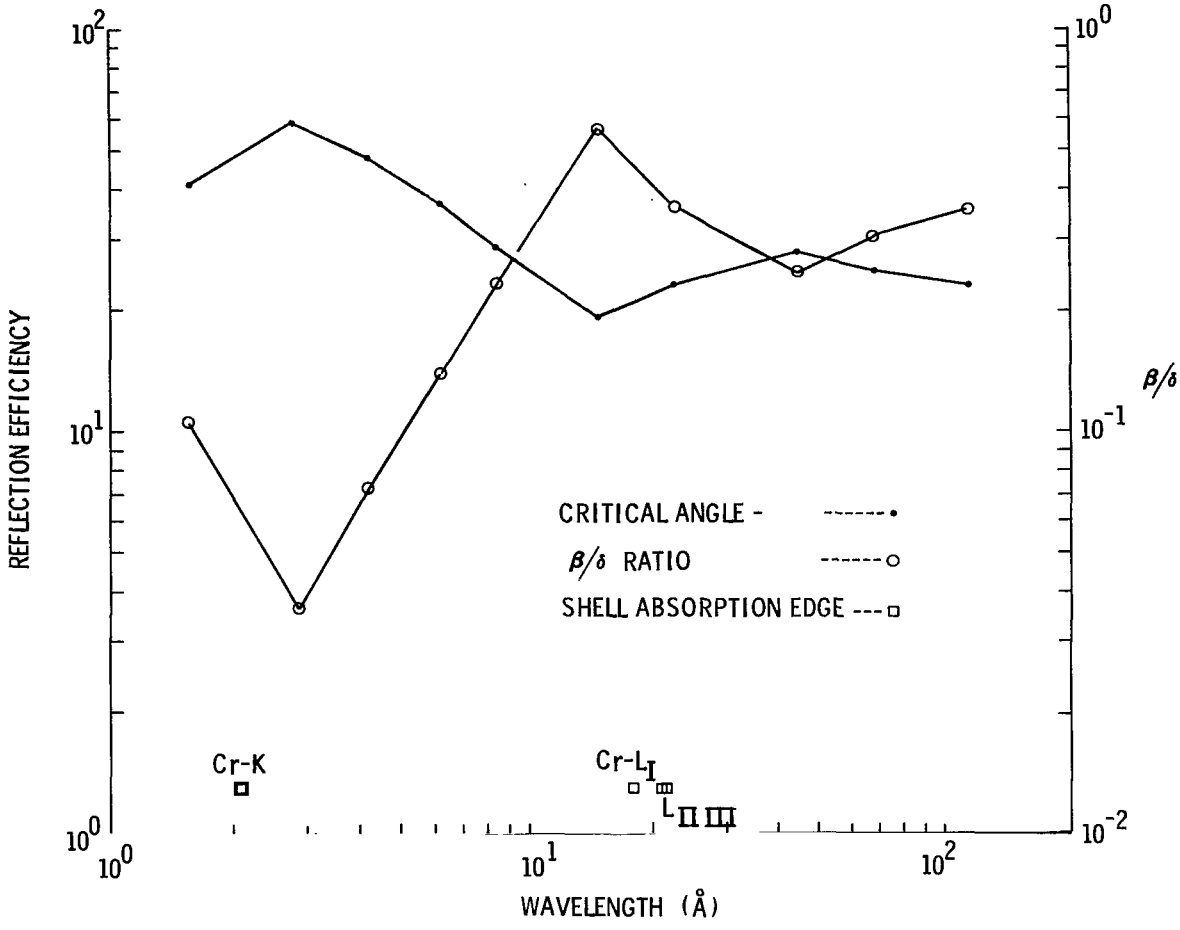

Figure 19. Critical angle, β/δ ratio, and shell absorption edge for chromium, $\lambda = 1.54$ Å to 113 Å.

reflection efficiency of Figures 20 through 23. The effect of the Be K-absorption edge at 111.6 Å is noted in curve I of Figure 21. It appears, when comparing Figures 22 and 23, that some of the absorption edges of the elements constituting smaller percentages may affect the shape of the theoretical curve. For example, silicon has two absorption edges, one at 6.74 Å and another at 83.4 Å. A comparison of these edges, the critical angles, and the β/δ ratios illustrates the shell influence that contributes to a decrease in the reflection efficiency.

TABLE 7. ATOMIC SHELL PARAMETERS OF BERYLLIUM, $\lambda = 8.34$ Å

Element	q	λ_q(Å)	P_q	g_q	Shell Term	Atom Term	Delta
Be	K	111.6	2.75	2.06	0.6536×10^{-1}	0.4271	0.1488×10^{-3}
BeO Be	K	111.6	2.75	2.06	0.6536×10^{-1}	0.4770×10^{-2}	0.1662×10^{-5}
O	K	23.3	2.75	1.55	0.2919		
O	L_I	518	2.00	1.60	-0.4147×10^{-3}		
O	$L_{II\,III}$	1780	2.50	5.40	0.3724×10^{-2}	0.1388×10^{-1}	0.4839×10^{-5}
C	K	43.6	2.75	1.45	0.1592		
	$L_{II\,III}$	1937	2.5	5.00	0.3049×10^{-2}	0.5325×10^{-3}	0.1855×10^{-6}
Fe	K	1.74	2.75	1.33	-1.357		
	L_I	14.65	2.00	1.37	-0.5039		
	L_{II}	17.19	2.50	1.87	0.9668×10^{-1}		
	L_{III}	17.50	2.50	4.24	0.2476		
	M_I	13.34	2.50	1.00	0.2508×10^{-1}		
	$M_{II\,III}$	229.5	2.50	4.95	0.6114×10^{-1}	0.4454×10^{-2}	0.1552×10^{-5}
Al	K	7.95	2.75	1.57	-3.894		
	L_I	105.3	2.00	1.35	-0.8479×10^{-2}		
	$L_{II\,III}$	170	2.50	6.97	0.1284	0.5443×10^{-2}	0.1896×10^{-5}
Mg	K	9.50	2.75	1.62	-1.661		
	L_I	38.68	2.00	1.30	-0.6139×10^{-1}		
	$L_{II\,III}$	24.12	2.50	7.02	0.8115×10^{-1}	0.2174×10^{-2}	0.7577×10^{-6}
Si	K	6.74	2.75	1.45	-2.278		
	L_I	83.2	2.00	1.55	-0.1562×10^{-1}		
	$L_{II\,III}$	124	2.50	5.00	0.1375		
	M_I	1550	2.50	2.00	0.1686×10^{-2}		
	$M_{II\,III}$	4130	2.50	2.00	0.4031×10^{-3}	0.9471×10^{-2}	0.3300×10^{-5}
						Delta Sum	0.1630×10^{-3}

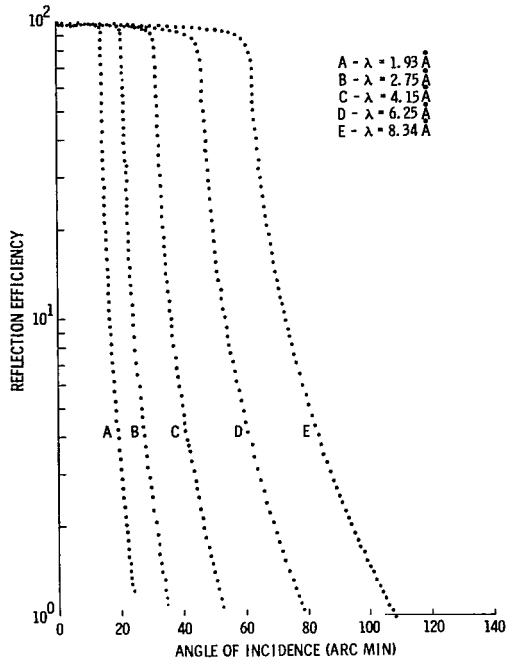

Figure 20. Reflection efficiency for beryllium, λ = 1.93 Å, 2.75 Å, 4.15 Å, 6.15 Å, and 8.34 Å.

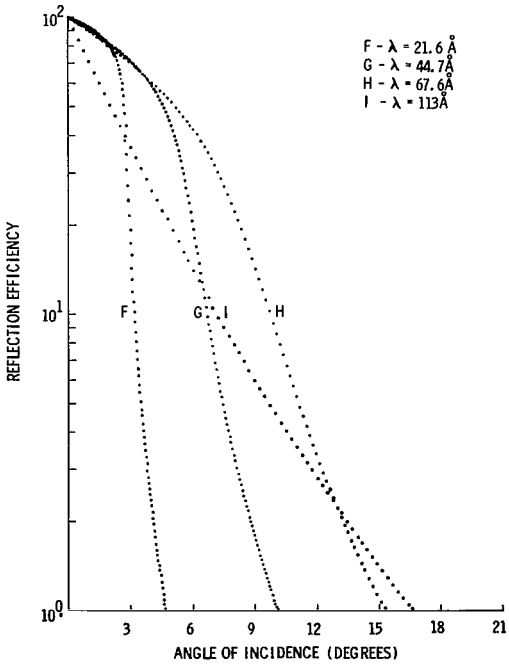

Figure 21. Reflection efficiency for beryllium, λ = 21.6 Å, 44.7 Å, 67.6 Å, and 113 Å.

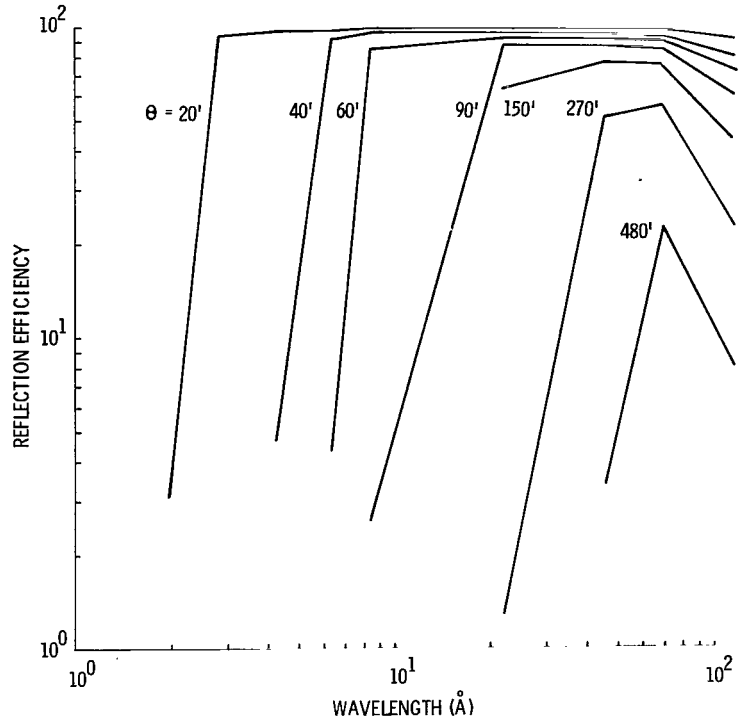

Figure 22. Theoretical reflection efficiency for beryllium, λ = 1.93 Å to 113 Å.

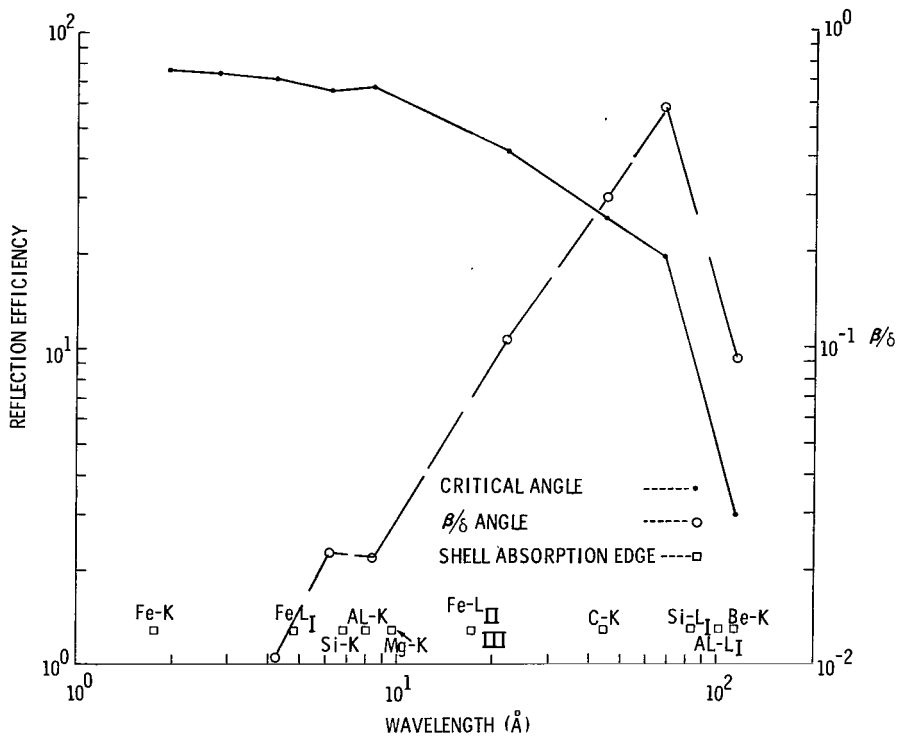

Figure 23. Critical angle, β/δ ratio, and shell absorption edge for beryllium, λ = 1.93 Å to 113 Å.

The critical angle and the δ-value were compared to those published by Schroeder, et al. [4]. They used equation (5) ($\Delta f_a = 0$) for their calculation of δ. A comparison is as follows:

		Reference 4
δ :	0.869×10^{-6}	0.84×10^{-6}
θ_c :	14.33 min	13.79 min

Gold

Gold, which has many atomic shells, was the fourth material studied. An assumption was made that the gold layer would be 1000 Å thick and coated on a fused silica substrate. While beryllium has one shell and an atomic number of 4, gold has many shells and an atomic number of 79. The first 16 shells of gold were combined into 8 (for calculation purposes) based on the similarity of their shell absorption edges (Table 8).

As the atomic number increases, so does the angle of incidence in X-ray reflection. An exception to this is around an absorption edge. A comparison of beryllium with gold follows:

Material	λ(Å)	Angle of Incidence (min)	Percent of Reflection
Be	8.34	63	50
Au/SiO_2	8.34	138	50
SiO_2	8.34	64	50

Figures 24 through 27 present the individual wavelengths for gold, and Figure 28 is a consolidation of Figures 24 through 27. The trend for these various angles of incidence indicates the effect of the shell absorption edge. Also, in Figure 29, the influence of the edges is seen in the critical angles and the β/δ ratio.

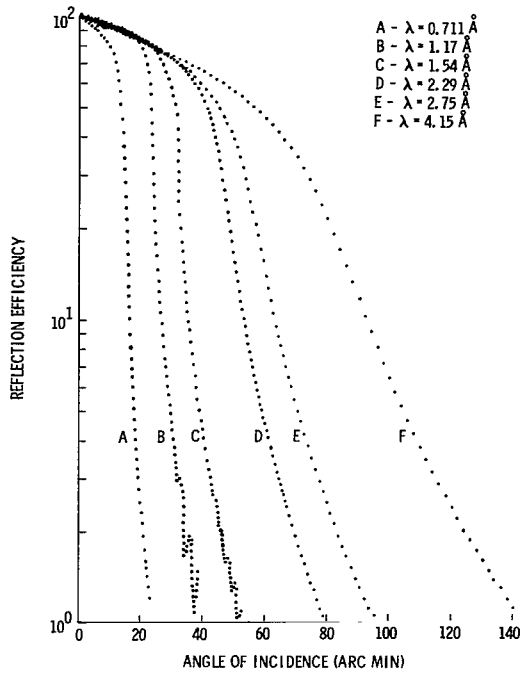

Figure 24. Reflection efficiency for gold, λ = 0.711 Å, 1.17 Å, 1.54 Å, 2.29 Å, 2.75 Å, and 4.15 Å.

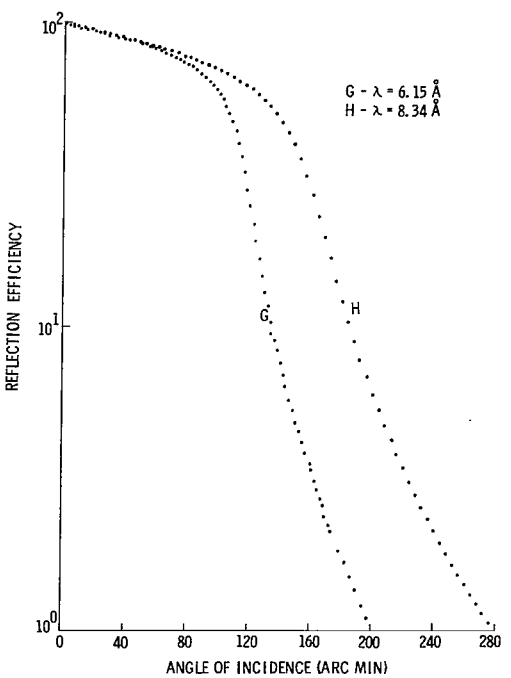

Figure 25. Reflection efficiency for gold, λ = 6.15 Å and 8.34 Å.

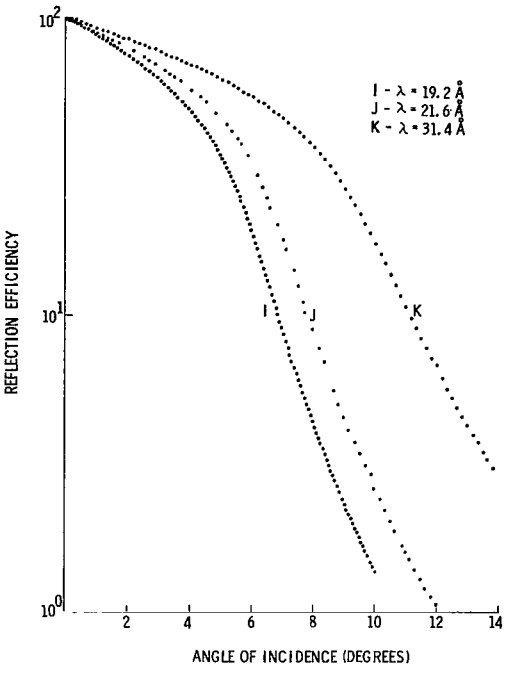

Figure 26. Reflection efficiency for gold, λ = 19.2 Å, 21.6 Å, and 31.4 Å.

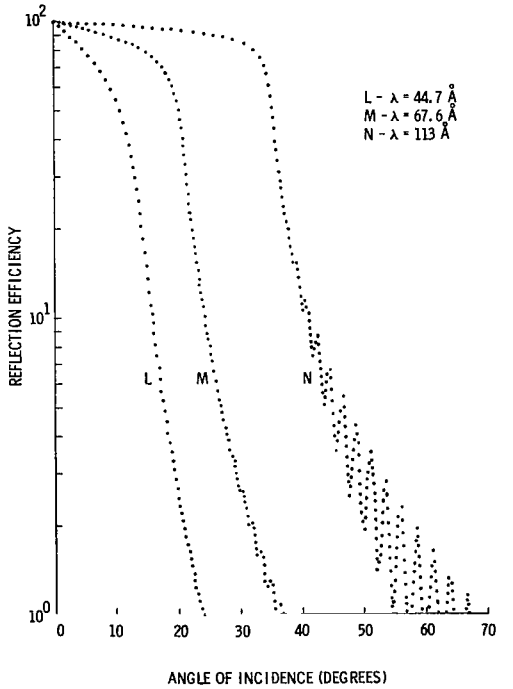

Figure 27. Reflection efficiency for gold, λ = 44.7 Å, 67.6 Å, and 113 Å.

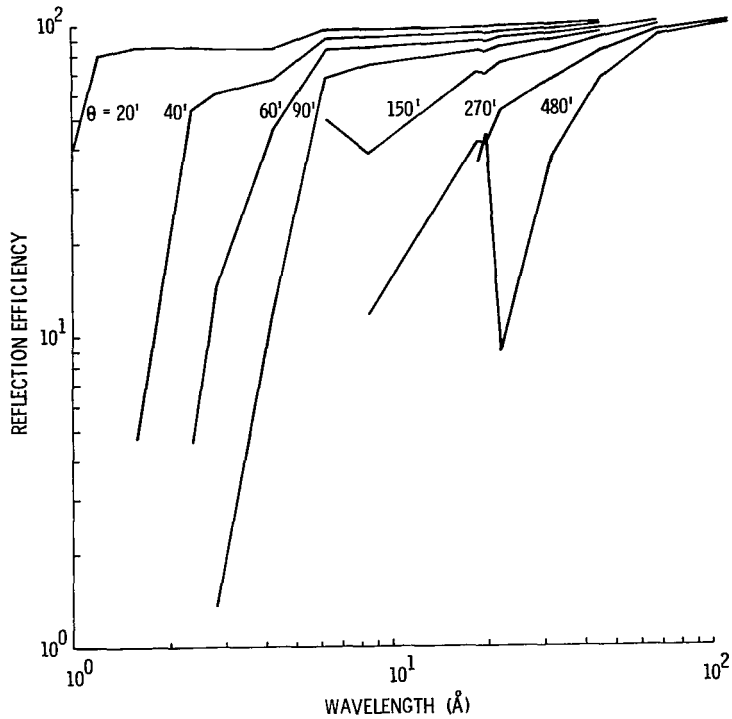

Figure 28. Theoretical reflection efficiency for gold, $\lambda = 0.711$ Å to 113 Å.

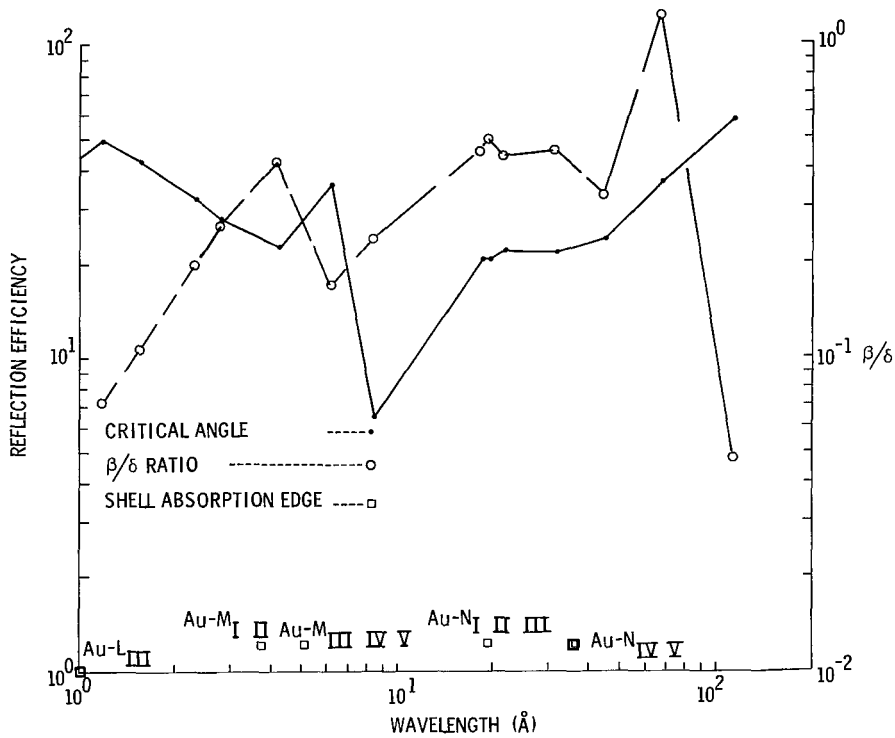

Figure 29. Critical angle, β/δ ratio, and shell absorption edge for gold, $\lambda = 0.711$ Å to 113 Å.

TABLE 8. ATOMIC SHELL PARAMETERS OF GOLD, $\lambda = 8.34$ Å

Element	q	λ_q (Å)	P_q	g_q	Shell Term	Atom Term
Au	K	0.1530	2.75	1.25	-1.250	
	L_I L_{II}	0.8830	2.42	1.16	-1.165	
	L_{III}	1.040	2.50	2.26	-2.275	
	M_I M_{II}	3.780	2.50	1.14	-1.255	
	M_{III} IV V	5.184	2.50	4.29	-5.246	
	N_I N_{II} N_{III}	19.44	2.50	1.39	0.1212	
	N_{IV} N_V	36.17	2.50	3.88	0.3865	
	N_{VI} VII	146.6	2.50	12.36	0.2750	0.3481
					Delta Sum	0.1067×10^{-2}

Fused Silica — Contaminated

A contaminant with a composition of $C_{28}H_{32}Si_3O_2$ was assumed to be coated as a single uniform layer on fused silica at a density of 1.0 g/cm^3. This chemical composition is similar to some of the diffusion pump fluids offered by various manufacturers.

Figure 30 is a demonstration of an increase in layer thickness of the contaminant in 25 Å increments and at an incident wavelength of 8.34 Å. The effect of the contaminant on the reflection efficiency for the 100 Å film is evident at θ slightly greater than θ_c and increases as θ increases. The contaminant effect on the reflection efficiency below 10 percent is predominant at a thickness from 20 to 100 Å. When the layer thickness of the contaminant is increased sufficiently, an interference peak occurs in the lower reflection efficiency region, or at large values of θ (Fig. 31). If desired, the relative

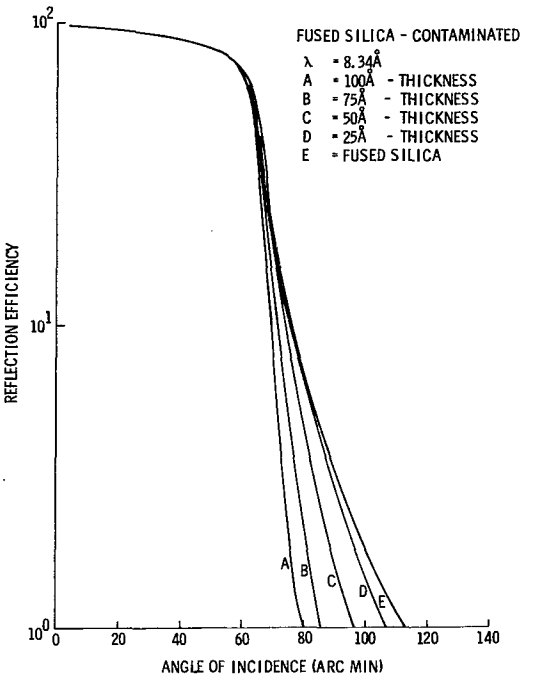

Figure 30. Reflection efficiency for fused silica, contaminated, $\lambda = 8.34$ Å, 25 Å to 100 Å film thickness.

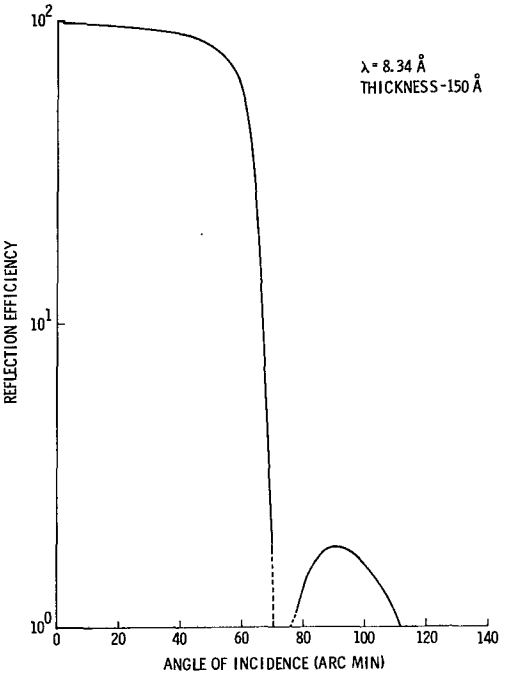

Figure 31. Reflection efficiency for fused silica, contaminated, $\lambda = 8.34$ Å, 150 Å film thickness.

position of the interference peaks can be utilized to approximate the thickness of the contaminant in the following manner:

$$\left(N - \frac{1}{2}\right)\lambda = 2d(\theta^2_{max} - 2\delta)^{1/2} \tag{13}$$

where

N = order number of successive maxima

d = film thickness

λ = wavelength of X-rays

θ_{max} = position of maximum (radian)

δ = deviation from unity of real part of refractive index.

Equation (13) is valid if $\theta > \theta_c$ and if the reflecting material is nonabsorbing. In the typically absorbing case, it is possible (depending upon precision available and accuracy desired) to approximate the thickness merely by replacing the $\lambda/2$ shift by a factor specifically characteristic and determined from the varying spacing of the interference peaks, represented as follows:

$$(N - K)\lambda = 2d(\theta^2_{max} - 2\delta)^{1/2} \quad , \tag{14}$$

where K = the numerical constant on the order of one-half.

Table 9 is a tabulation of the interference peaks at the angle of incidence and the reflection efficiency at which they occur. From this table it appears that as the thickness of the contaminant layer increases, the number of interference peaks also increases, occurring at smaller values of θ and therefore at a higher X-ray reflection. As the layer thickness increases from 250 to 1000 Å and the number of interference peaks increases, the interference effect of the film on the shape of the reflection efficiency curve becomes more constant compared to the changing effect in the thinner films. For a layer thickness of 150 to 1000 Å (Figs. 31 through 39), the majority of these peaks occur from 52 to 74 min angle of incidence. In Figure 35 the contaminant density was varied ± 0.1 g/cm^3 to illustrate the effect on the efficiency and the interference peaks.

TABLE 9. INTERFERENCE PEAKS

Thickness (Å)	θ (min)	Reflection Efficiency (%)
150 (Fig. 31)	90	1.8
175 (Fig. 32)	80	3.4
200 (Fig. 33)	70	6.0
225 (Fig. 34)	70	10.0
250 (Fig. 35)	64	A - 12 B - 18 C - 28
375 (Fig. 36)	62	46.0
	88	3.0
500 (Fig. 37)	58	50.0
	72	9.0
	98	1.7
750 (Fig. 38)	54	47.0
	62	35.0
	74	7.9
	90	2.5
	106	1.1
1000	52	41.0
	58	38.0
	64	22.0
	74	6.6
	86	3.0
	98	1.5

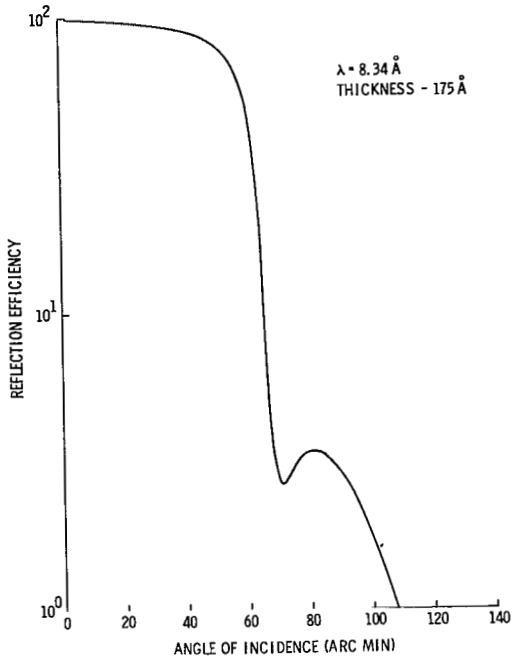

Figure 32. Reflection efficiency for fused silica, contaminated, λ = 8.34 Å, 175 Å film thickness.

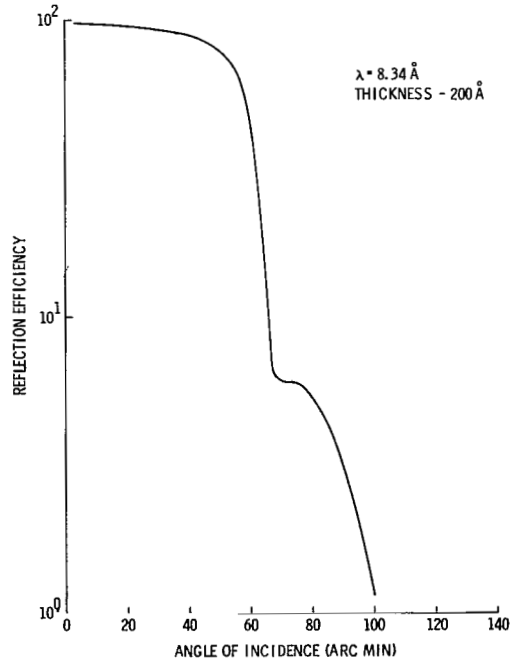

Figure 33. Reflection efficiency for fused silica, contaminated, λ = 8.34 Å, 200 Å film thickness.

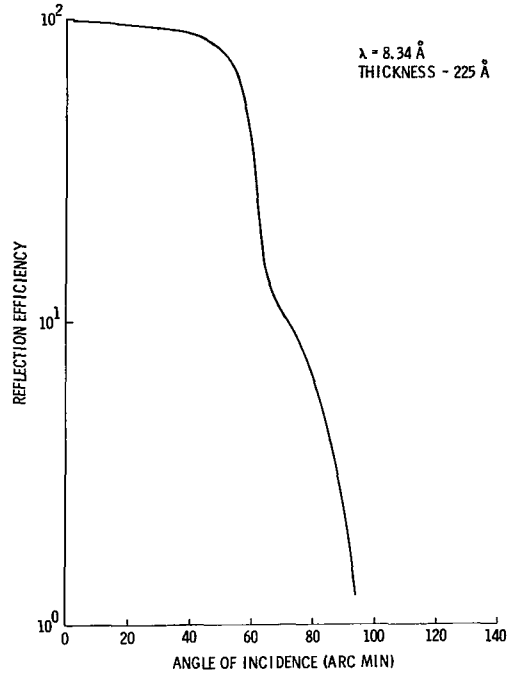

Figure 34. Reflection efficiency for fused silica, contaminated, $\lambda = 8.34$ Å, 225 Å film thickness.

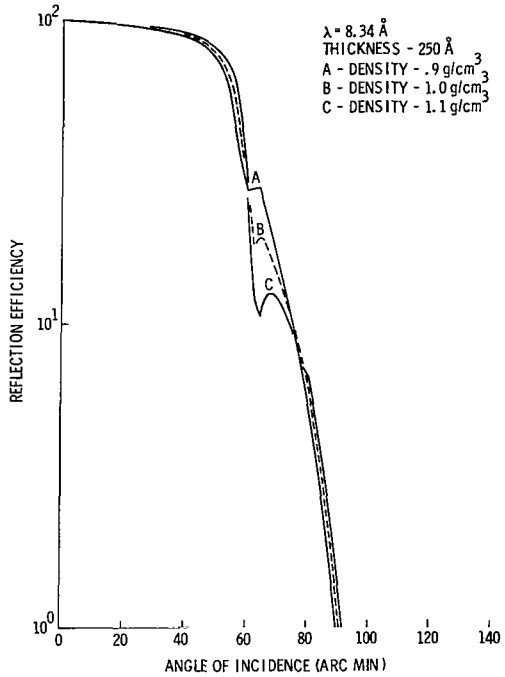

Figure 35. Reflection efficiency for fused silica, contaminated, $\lambda = 8.34$ Å, 250 Å film thickness.

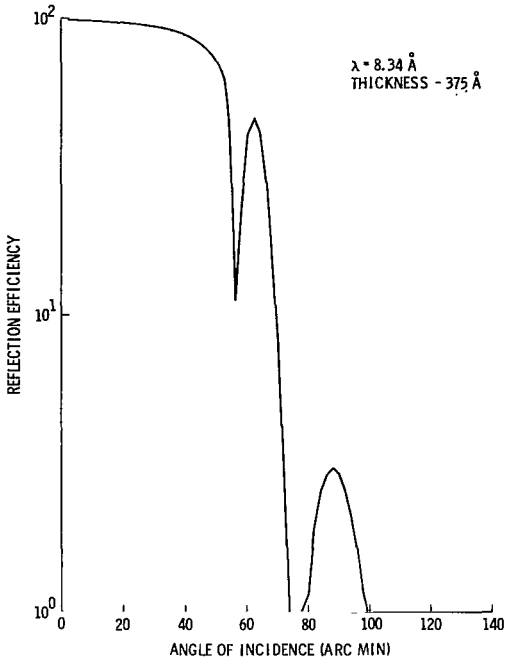

Figure 36. Reflection efficiency for fused silica, contaminated, λ = 8.34 Å, 375 Å film thickness.

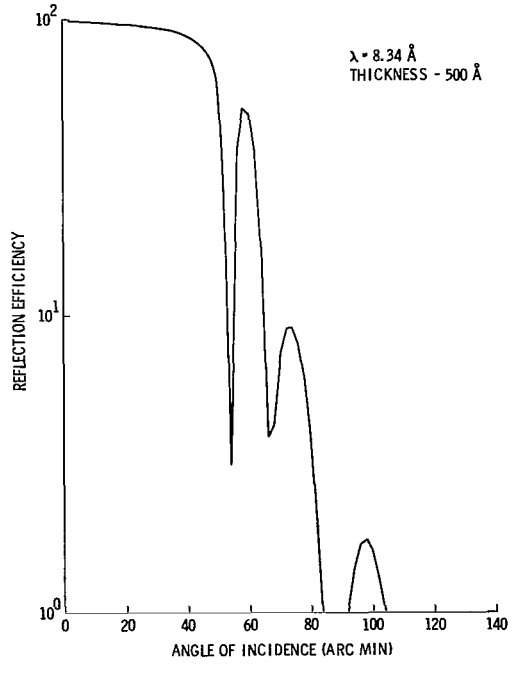

Figure 37. Reflection efficiency for fused silica, contaminated, λ = 8.34 Å, 500 Å film thickness.

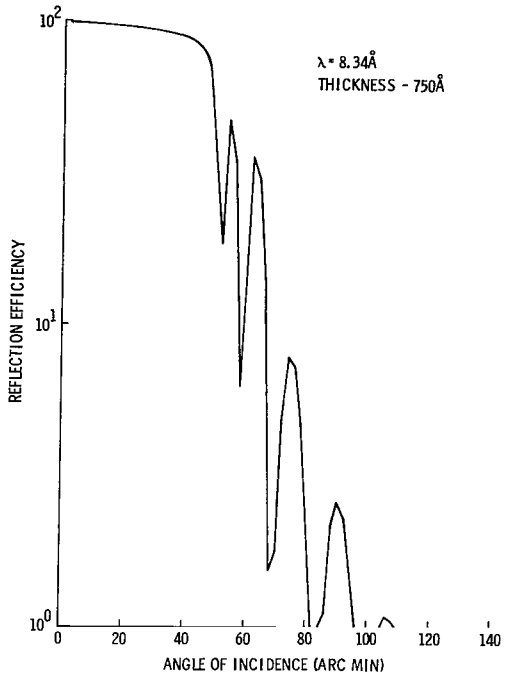

Figure 38. Reflection efficiency for fused silica, contaminated, λ = 8.34 Å, 750 Å film thickness.

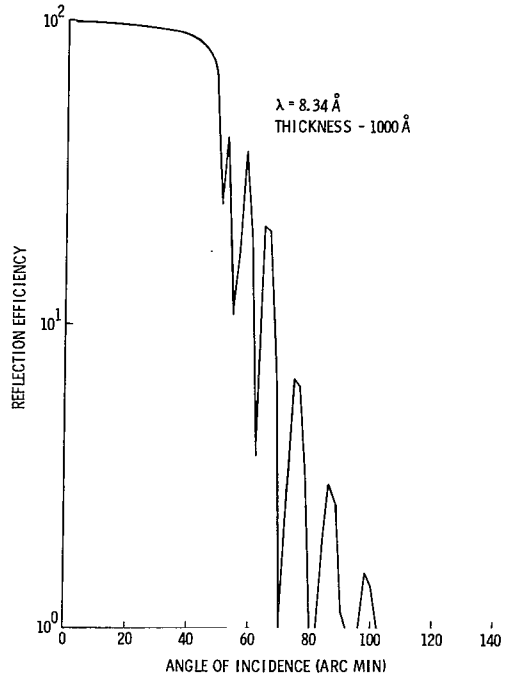

Figure 39. Reflection efficiency for fused silica, contaminated, λ = 8.34 Å, 1000 Å film thickness.

Figure 40 is a summation of Figures 30 through 39. For angles of incidence of 20, 40, and 44 min there is very little decrease in reflection efficiency from 25 to 1000 Å layer thickness. As the angle of incidence increases per layer thickness increase, the general trend is a decrease in X-ray reflection efficiency at 8.34 Å.

Figures 41 through 43 are examples of a 50 Å layer thickness contaminant with incident radiation from 1.54 to 113 Å. The effect of the contaminant at these wavelengths can be determined by comparison with Figures 7 through 11. Figure 44 is a consolidation of Figures 41 through 43, and Figure 45 is a graph of the critical angles, β/δ ratios, and the shell absorption edges.

SUMMARY

The theor lection of X-rays has been demonstrated in this heir effect necessary to generate these data have been identified. Some of the quantities are the atomic number, atomic weight, density, thickness, and chemical composition of the materials. Also, the presentation of the X-ray reflection efficiency curves is based on atomic considerations.

It was also noted that both the literature values for the oscillator model parameters and the combinations of these values which result in X-ray index of refraction are of a nonunique nature. In terms of the literature values, the nonuniqueness concerns both oscillator model values and the associated index of refraction, resulting in an extensive lack of valid comparisons in the literature. The multiplicity of model parameter combinations (yielding identical indices of refraction) necessitated considerations which, with slight modification of the existing computer programs, can result in the generation of X-ray reflection efficiency from a priori considerations. It was also noted that, given existing experimental inaccuracies, further refinement of the approach of Cromer is unnecessary from a comparison standpoint. In many cases, however, to achieve valid comparisons between experimental and theoretical X-ray reflection efficiency curves or to generate valid efficiency predictions, it is necessary to utilize the oscillator model correction (equation) and the more precise parameters (a course which is not common in the literature).

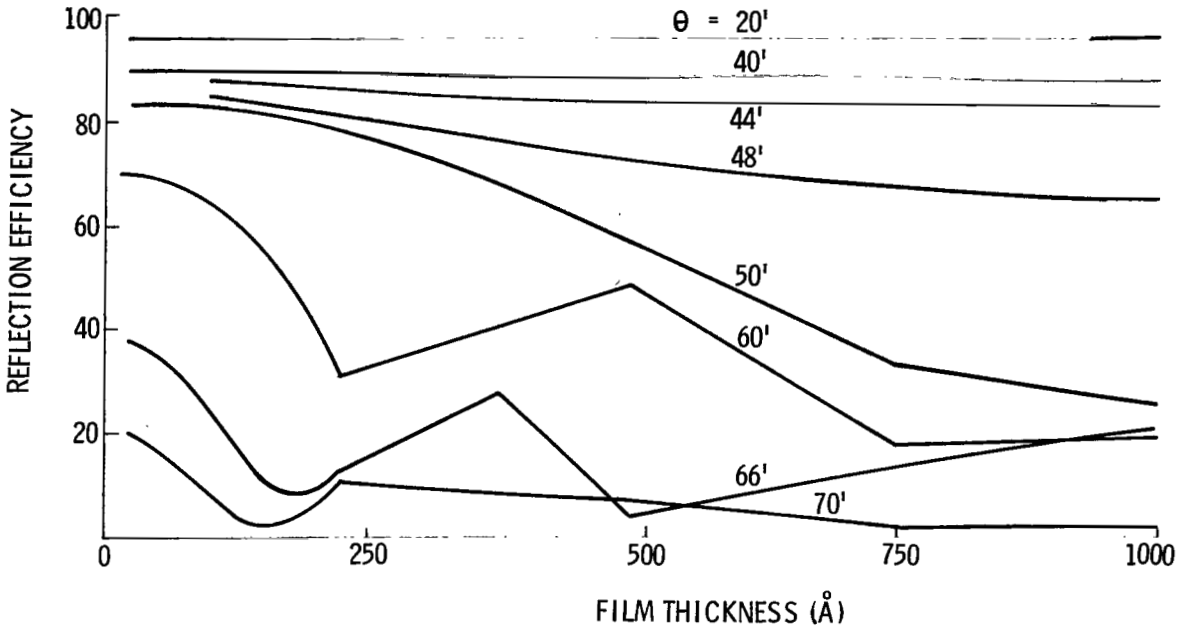

Figure 40. Reflection efficiency for fused silica, contaminated, $\lambda = 8.34$ Å, 25 Å to 1000 Å film thickness, θ = 20 min to 70 min angle of incidence.

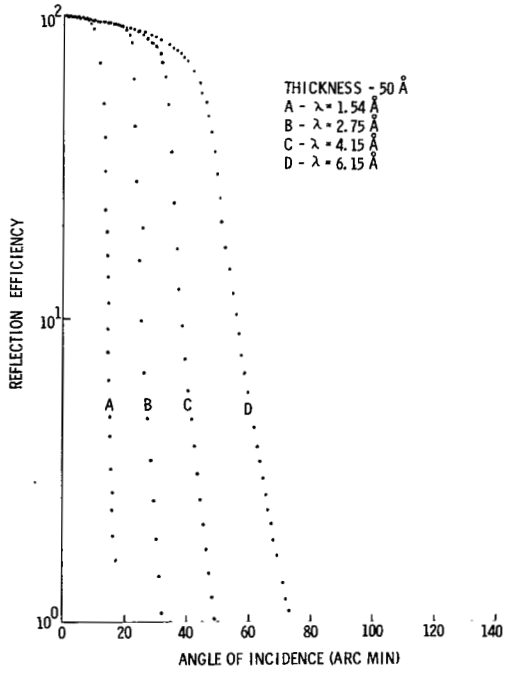

Figure 41. Reflection efficiency for fused silica, contaminated, $\lambda = 1.54$ Å, 2.75 Å, 4.15 Å, and 6.15 Å.

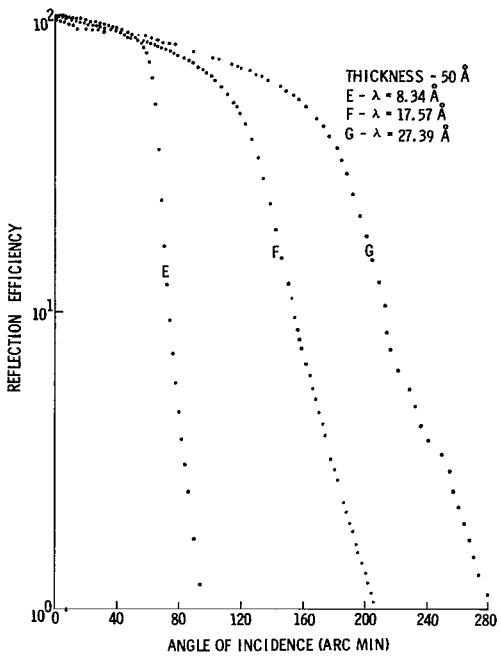

Figure 42. Reflection efficiency for fused silica, contaminated, λ = 8.34 Å, 17.57 Å, and 27.39 Å.

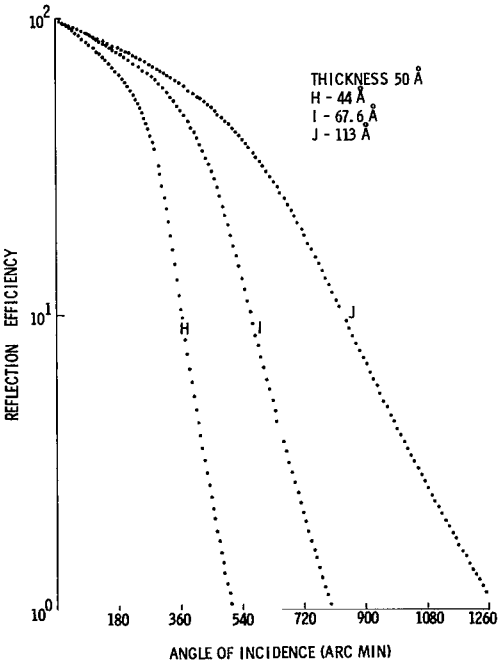

Figure 43. Reflection efficiency for fused silica, contaminated, λ = 44 Å, 67.6 Å, and 113 Å.

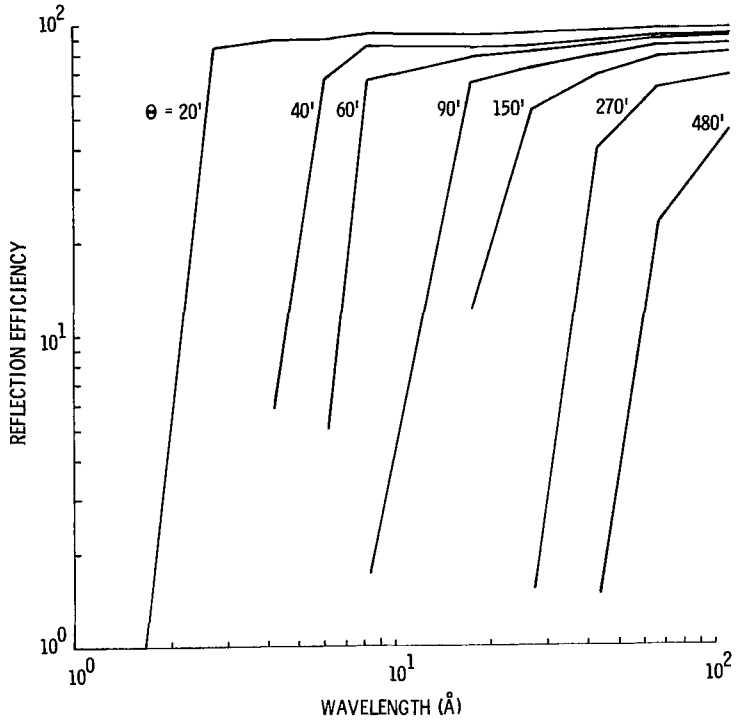

Figure 44. Theoretical reflection efficiency for fused silica, contaminated, λ = 1.54 Å to 113 Å.

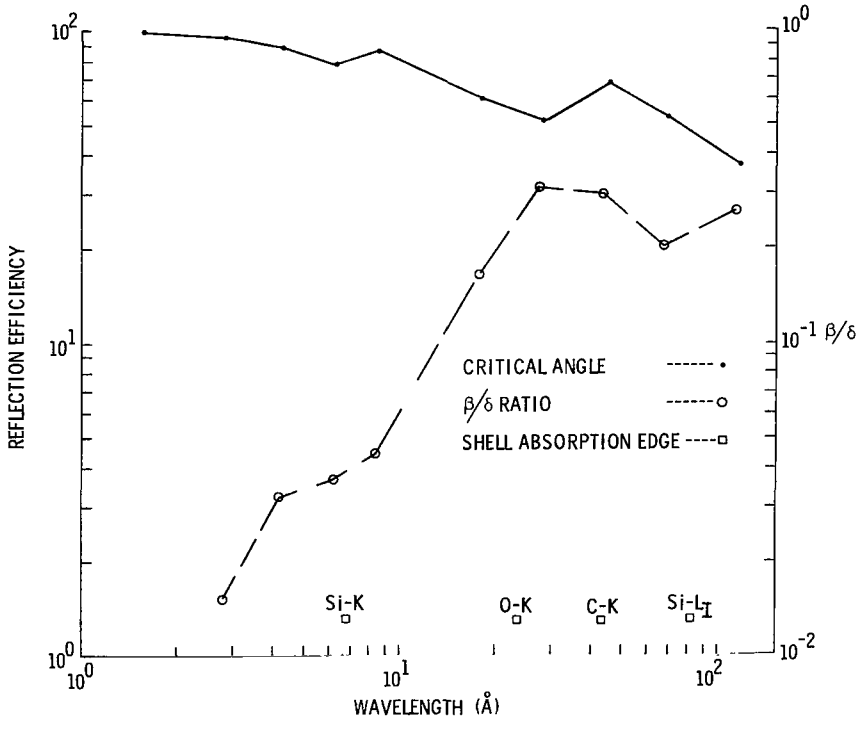

Figure 45. Critical angle, β/δ ratio, and shell absorption edge for fused silica, contaminated, λ = 1.54 Å to 113 Å.

From a macroscopic point of view, this report focused primarily upon the thickness and density of a deposited material, applicable to both mirror coating and contamination.

The influence of density on both the parameters of reflection efficiency and the reflection efficiency curve itself is significant. In cases where the density of the material is unknown, the X-ray characteristics can be used with comparison and controlled testing for accurate prediction of a controlled deposition process.

If the thin film deposited on a reflecting surface is of a contaminant type, various interference peaks can occur in relation to the thickness. The theoretical calculations have the capability for predictions involving a range from a single element to multiple chemical element materials; thus, all elements contribute to the reflection of the X-rays.

REFERENCES

1. Compton, A. H. and Allison, S. K.: X-Rays in Theory and Experiment. D. Van Nostrand Company, Inc., 1935.

2. Parratt, L. G. and Hempstead, C. F.: Anomalous Dispersion and Scattering of X-Rays. Physical Review, vol. 94, no. 6, 1954, pp. 1593-1600.

3. Lightweight X-Ray Telescopes. Perkin-Elmer Corporation, Final Report, Contract NAS8-20727, 1969.

4. Schroeder, J. B. and Klimasewski, R. G.: Scatter from X-Ray Reflecting Surfaces. Applied Optics, vol. 7, 1968, pp. 1921-1927.

5. Bearden, J. A.: X-Ray Wavelengths and X-Ray Atomic Energy Levels. NSRDS-NBS 14, 1967.

6. Neal, W. R., Zehnpfennig, T. F., and Reidy, W. P.: Design, Manufacture and Install Sample Holder in X-Ray Reflectometer and Perform Data Analysis of Results. Visidyne, Inc., Contract NAS8-27605, July 1972.

7. Cromer, D. T.: Anomalous Dispersion Corrections Computed from Self-Consistent Field Relativistic Dirac-Slater Wave Functions. Acta Cryst., vol. 18, 1965, pp. 17-23.

8. West, R. C.: Handbook of Chemistry and Physics. 54th edition, CRC Press, Cleveland, Ohio, 1973-1974.

9. Theisen, R. and Vollath, D.: Tables of X-Ray Mass Attenuation Coefficients. Verlag Stahleisen M. B. H., Dusseldorf, 1967.

10. Henke, B. L. and Ebisu, E. S.: Mass Absorption Coefficients. Advances in X-Ray Analysis, vol. 17, 1973, pp. 187-213.

11. James, R. W.: The Optical Principles of the Diffraction of X-Rays. The Crystalline State, Vol. II. Cornell University Press, 1965, pp. 159-161.

REFERENCES (Concluded)

12. Reiser, L. M., Jr.: Reflection of X-Rays and the Reflection Microscope. X-Ray Optics and X-Ray Microanalysis, W. H. Pattee, V. E. Cosslett, and A. Engstrom, eds., Academic Press, New York and London, 1963, pp. 195-209.

13. Reiser, L. M., Jr.: Reflection of X-Rays from Condensed Metal Films. J. Opt. Soc. Am., vol. 47, no. 11, November 1957, pp. 987-994.

14. Scott, N. J.: Study of Thin Vacuum Deposited Copper Films by X-Ray Total Reflection. AFOSR-TN-57-779, ASTIA AD 148-010, Technical Report No. 11, 1957.

15. Duncan, R. C. and Parratt, L. G.: A Study of Evaporated Aluminum Films by X-Ray Total Reflection. AFOSR-TN-58-680, ASTIA AD 162-212, Technical Report No. 13, 1958.

16. Dershem, E. and Shein, M.: The Absorption of the K Line of Carbon in Various Gases and Its Dependence upon Atomic Number. Physical Review, vol. 37, May 15, 1931, pp. 1238-1251.

17. Hendrick, R. W.: Spectral Reflectance of Solids for Aluminum K Radiation. J. Opt. Soc. of Am., vol. 47, no. 2, 1957, pp. 165-171.

18. Johnson, G. L. and Wuerker, R. F.: Reflectance of Carbon-K and Beryllium-K Wavelengths. X-Ray Optics and X-Ray Microanalysis, W. H. Pattee, V. E. Cosslett, and A. Engstrom, eds., Academic Press, New York and London, 1963, pp. 229-239.

"The aeronautical and space activities of the United States shall be conducted so as to contribute . . . to the expansion of human knowledge of phenomena in the atmosphere and space. The Administration shall provide for the widest practicable and appropriate dissemination of information concerning its activities and the results thereof."

—NATIONAL AERONAUTICS AND SPACE ACT OF 1958

NASA SCIENTIFIC AND TECHNICAL PUBLICATIONS

TECHNICAL REPORTS: Scientific and technical information considered important, complete, and a lasting contribution to existing knowledge.

TECHNICAL NOTES: Information less broad in scope but nevertheless of importance as a contribution to existing knowledge.

TECHNICAL MEMORANDUMS: Information receiving limited distribution because of preliminary data, security classification, or other reasons. Also includes conference proceedings with either limited or unlimited distribution.

CONTRACTOR REPORTS: Scientific and technical information generated under a NASA contract or grant and considered an important contribution to existing knowledge.

TECHNICAL TRANSLATIONS: Information published in a foreign language considered to merit NASA distribution in English.

SPECIAL PUBLICATIONS: Information derived from or of value to NASA activities. Publications include final reports of major projects, monographs, data compilations, handbooks, sourcebooks, and special bibliographies.

TECHNOLOGY UTILIZATION PUBLICATIONS: Information on technology used by NASA that may be of particular interest in commercial and other non-aerospace applications. Publications include Tech Briefs, Technology Utilization Reports and Technology Surveys.

Details on the availability of these publications may be obtained from:

SCIENTIFIC AND TECHNICAL INFORMATION OFFICE

NATIONAL AERONAUTICS AND SPACE ADMINISTRATION

Washington, D.C. 20546